Fine-scale hydrodynamics influence the spatio-temporal distribution of harbour porpoises at a coastal hotspot

A.R. Jones [a,*], P. Hosegood [b], R.B. Wynn [a], M.N. De Boer [c,d], S. Butler-Cowdry [a], C.B. Embling [e,f]

[a] National Oceanography Centre – Southampton, European Way, Southampton SO14 3ZH, UK
[b] University of Plymouth, School of Marine Science and Engineering (Faculty of Science and Technology), Reynolds Building, Drake Circus PL4 8AA, UK
[c] Wageningen IMARES, Institute for Marine Resources and Ecosystem Studies, PO Box 167, 1790 AD Den Burg, The Netherlands
[d] Marine Discovery Penzance, Shed 5, Albert Pier, Penzance Harbour, Penzance TR18 2LL, UK
[e] Centre for Ecology and Conservation, University of Exeter, Cornwall Campus, Penryn TR10 9EZ, UK
[f] Marine Institute, University of Plymouth, Marine Building, Drake Circus PL4 8AA, UK

ARTICLE INFO

ABSTRACT

The coastal Runnelstone Reef, off southwest Cornwall (UK), is characterised by complex topography and strong tidal flows and is a known high-density site for harbour porpoise (*Phocoena phocoena*); a European protected species. Using a multidisciplinary dataset including: porpoise sightings from a multi-year land-based survey, Acoustic Doppler Current Profiling (ADCP), vertical profiling of water properties and high-resolution bathymetry; we investigate how interactions between tidal flow and topography drive the fine-scale porpoise spatio-temporal distribution at the site. Porpoise sightings were distributed non-uniformly within the survey area with highest sighting density recorded in areas with steep slopes and moderate depths. Greater numbers of sightings were recorded during strong westward (ebbing) tidal flows compared to strong eastward (flooding) flows and slack water periods. ADCP and Conductivity Temperature Depth (CTD) data identified fine-scale hydrodynamic features, associated with cross-reef tidal flows in the sections of the survey area with the highest recorded densities of porpoises. We observed layered, vertically sheared flows that were susceptible to the generation of turbulence by shear instability. Additionally, the intense, oscillatory near surface currents led to hydraulically controlled flow that transitioned from subcritical to supercritical conditions; indicating that highly turbulent and energetic hydraulic jumps were generated along the eastern and western slopes of the reef. The depression and release of isopycnals in the lee of the reef during cross-reef flows revealed that the flow released lee waves during upslope currents at specific phases of the tidal cycle when the highest sighting rates were recorded. The results of this unique, fine-scale field study provide new insights into specific hydrodynamic features, produced through tidal forcing, that may be important for creating predictable foraging opportunities for porpoises at a local scale. Information on the functional mechanisms linking porpoise distribution to static and dynamic physical habitat variables is extremely valuable to the monitoring and management of the species within the context of European conservation policies and marine renewable energy infrastructure development.

© 2014 The Authors. Published by Elsevier Ltd. This is an open access article under the CC BY license (http://creativecommons.org/licenses/by/3.0/).

Introduction

Marine megavertebrates are noted for their wide-ranging behaviour, but often concentrate within spatially constrained areas (e.g. Sims, 2003; Kai et al., 2009), referred to as 'hotspots' (Myers, 1990). The mechanism driving animal aggregations at hotspots is likely to be based on foraging decisions made in response to meso- and fine-scale environmental cues (Stephens and Krebs, 1986; Russell et al., 1992; Sims et al., 2008). By examining the distribution of a species in time and space, at a range of scales, we can improve our understanding of the species' interaction with its environment (Fauchald and Erikstad, 2002; Bertrand et al., 2008; Embling et al., 2012). This is particularly important for spatial management and conservation of threatened marine megavertebrates, such as the harbour porpoise *Phocoena phocoena*. A better understanding of the mechanisms underlying the links between porpoise distribution and physical habitat will aid in protected area site selection, as well as improving our understanding of potential anthropogenic impacts, e.g. proposed marine renewable energy infrastructure (Dolman and Simmonds, 2010; Witt et al., 2012).

* Corresponding author. Current address: The Environment Institute & School of Ocean and Earth Sciences, University of Adelaide, South Australia 5005, Australia. Tel.: +61 (0)8 8313 2243.
  E-mail address: alice.jones01@adelaide.edu.au (A.R. Jones).

Harbour porpoises are small cetaceans, which must feed regularly in order to fulfil their energetic requirements. As a result they cannot stray far from areas containing reliable prey resources (Brodie, 1995; Koopman, 1998; Santos et al., 2004; Lockyer, 2007), and the ability to react to predictable oceanographic and hydrodynamic drivers of prey availability will greatly reduce foraging costs. Broad-scale studies show that the distribution of harbour porpoises is directly influenced by the distribution of prey (e.g. Read and Westgate, 1997; Herr et al., 2009; Sveegaard, 2011) and indirectly affected by both static and dynamic environmental variables that are hypothesised to predictably influence prey distribution or foraging efficiency, such as water depth, topography, substrate, tidal flow, fronts, stratification, turbulence, and time of day (e.g. Watts and Gaskin, 1985; Johnston et al., 2005; Embling et al., 2010; Scott et al., 2010; Mikkelsen et al., 2013). However, there are no known studies investigating the fine-scale bio-physical mechanisms linking physical habitat variables to increased harbour porpoise densities, due to the rarity of the quantitative, fine-scale physical and biological data required to carry out robust investigations of these links.

Harbour porpoises have a wide coastal distribution around the UK (Reid et al., 2003; Hammond et al., 2013), making them a suitable focus species for land-based surveys. Sites around the coast of southwest England have previously been identified as hotspots for harbour porpoise (Northridge et al., 1995; Hammond, 2006; Brereton et al., 2007), with a number of studies specifically highlighting the regional importance of the Runnelstone Reef in southwest Cornwall (Leeney et al., 2008; Pikesley et al., 2012); not only in the summer months, but also throughout the winter (Evans et al., 2003; De Boer and Saulino, 2008). Using new high-resolution bathymetric data, we have been able to identify that the Runnelstone Reef site is a regionally unique bathymetric feature.

In light of the potential bio-physical links suggested by previous research, and the conservation and management policies pertaining to the species in the UK; this multidisciplinary study examines the effect of fine-scale physical habitat on harbour porpoise distribution. We investigate the drivers of porpoise distribution patterns using sightings recorded in an effort-based visual survey from a land-based watchpoint overlooking the Runnelstone Reef. The collection of co-located, high-resolution data on static and dynamic physical habitat variables, such as Acoustic Doppler Current Profiling (ADCP), water property profiles, and 1-m resolution bathymetry data, has provided a unique and timely opportunity to investigate the fine-scale spatial (~600 m resolution) and temporal (hourly resolution) distribution of harbour porpoises at a known hotspot in relation to hydrodynamics and interactions between tide and topography at the site. The main aims of the study were threefold: (1) to examine whether the spatial distribution of harbour porpoise sightings was linked to topographic features within the study area, (2) to collect high-resolution data on the physical marine environment at the study site, and (3) to investigate the spatio-temporal distribution of porpoise sightings in relation to tidal flow regime and fine-scale hydrodynamics.

Materials and methods

Study area

Survey data were collected from a land-based watchpoint on a south-facing headland (Gwennap Head) at ~30 m above mean sea level, at the southwest tip of the UK mainland (50°02′ 06.29″N 005°40′ 45.66″W). The watchpoint has an almost 180° field of view from east to west, directly overlooking the tidally dominated Runnelstone Reef (Fig. 1). The characteristics of the Runnelstone Reef create a challenging environment for data collection. Commercial

fishing activities in the area restrict the strategic mooring of large arrays of acoustic monitoring equipment, and the site is wind exposed and tidally dominated, which precludes regular boat-based transect surveys at an appropriately fine scale. This results in land-based observation surveys being the most effective, and practical, method for intensive fine-scale monitoring of the distribution of porpoises at this regionally important site.

The Runnelstone Reef is a roughly horseshoe-shaped bedrock platform with an average depth of approximately 15 m out to 1.6 km, where it shallows at its southern edge, forming several upstanding pinnacles that come to within a few metres of the surface. Beyond the pinnacles, water depth drops sharply to >60 m (Fig. 1). To the east and west sides of the reef the seafloor slopes away gently and depth increases gradually. Two high-resolution multi-beam bathymetry datasets were combined to create a full bathymetric map of the survey area (Fig. 1). Inshore data (up to ~2 km offshore), at a resolution of 1 m, were collected by the Plymouth Coastal Observatory as part of the Southwest Regional Coastal Monitoring Programme (© Teignbridge District Council), and provided by the Channel Coastal Observatory. Data from further offshore (12 m resolution) were collected as part of the Maritime and Coastguard Agency (MCA) Civil Hydrography Programme (CHP) (© Crown Copyright) and are released under the Open Government Licence.

Broad-scale tidal data from Admiralty Charts show that water is driven around the headland reef by the tidal current as it enters and exits the western English Channel during the semi-diurnal tidal regime. The tidal flow through the survey area is westward (i.e. flowing out of the Channel) for the majority of the semi-diurnal cycle. Eastwards flow (i.e. into the Channel) occurs for only ~3 h per tidal cycle, between approximately 1 h before, to 2 h after high water (HW). Tidal range varies from ~1.5 m during neap tides to ~5.5 m during spring tides.

Visual surveys

Visual monitoring data were collected between 15th July and 15th October 2007–2010. The survey period was defined by the migration season of seabirds and other marine megavertebrates, which were also monitored in the multi-species survey. Observations were carried out through the full daylight period each day; this intensive constant-effort design enabled investigation of fine-scale temporal patterns in the survey data. A 2-h break was taken each day between 1200 and 1400 h, to prevent observer fatigue and avoid the period of highest glare. Observers working in pairs, with one core observer and one supporting observer. The core observers (N = 29 over the 4-year period) were skilled in surveying for seabirds and cetaceans, with prior field experience of identifying the target species. Selection priority was given to supporting observers who had previous marine wildlife survey experience.

Observers applied continuous search effort using 8× or 10× magnification binoculars, with naked-eye and telescope (20–30× magnification) scans of the survey area to ensure even surveillance of the near and far fields. Telescopes were also used to ensure species ID and record group size. There was rotation of survey effort between observers and regular breaks were encouraged, whilst always maintaining at least two observers 'on watch'.

Harbour porpoise sighting records always included date, time, number of animals, movement direction and an estimate of distance and direction from the watchpoint to the point of first sighting (with subsequent sighting positions also recorded where possible). Best practice was to record direction using a compass, but on occasion a cardinal direction was used. The Runnelstone buoy was an obvious reference point, at approximately 1.6 km from the observation watchpoint, on a bearing of 170° (Fig. 1). Data
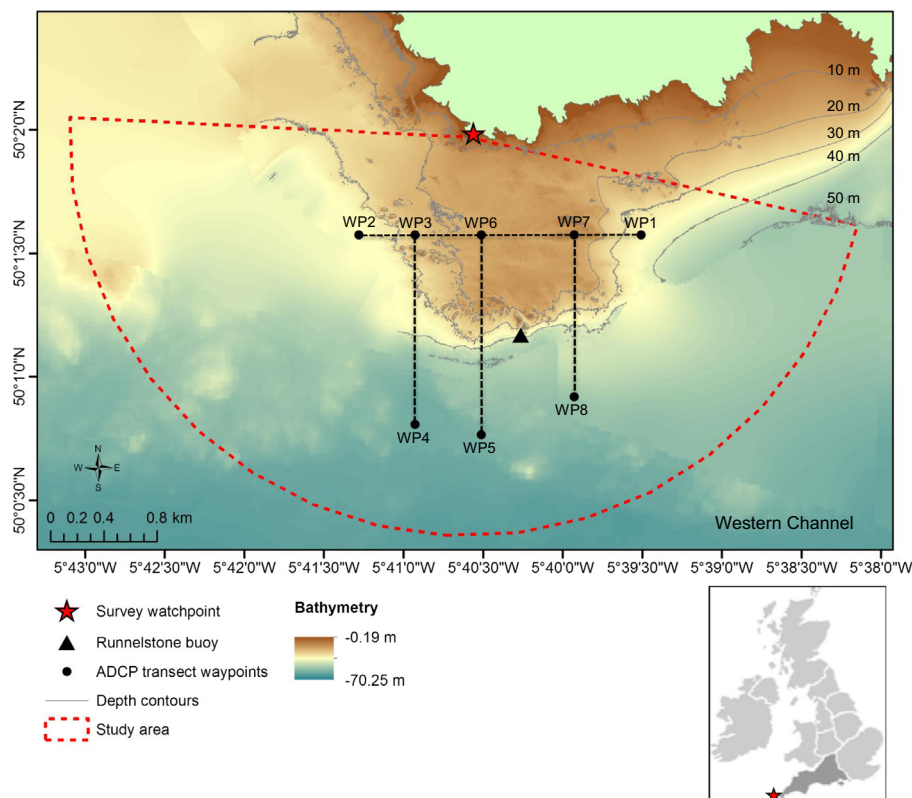
Fig. 1. Overview map of the study site off southwest Cornwall (UK) showing survey area extent and ADCP survey tracklines and waypoints. The bathymetry data has been regridded at a resolution of 12-m. Waypoints where CTD data were collected are indicated by red filled circles. Note the steep southern margin of the reef, and associated pinnacles immediately inshore of the Runnel Stone buoy (filled black triangle). (For interpretation of the references to colour in this figure legend, the reader is referred to the web version of this article.)

on survey conditions were recorded hourly, these included Beaufort sea state, visibility, cloud cover and glare.

Estimating error in sighting position estimates

Distance estimation was tested for two of the primary observers (jointly responsible for ~40% of total survey effort), in an attempt to constrain potential location errors associated with visually estimating positions of porpoises. Error tests were undertaken on two occasions, in October 2010 and January 2011. In the first test, observer-estimated positions of a boat were compared to the true position collected with an onboard GPS (2 observers, $N = 60$). During the second test (one observer, $N = 22$), visual estimates of the position of porpoises were compared to positions recorded using a surveyor's theodolite (Leica FlexLine TS02 Total Station). In both cases, observer estimates and 'true' positions were plotted in a GIS and the distance between them was calculated. The mean error across all tests ($N = 82$ position estimates by 2 observers) was 281 m (test 1 mean error = 320 m, SD = 141; test 2 mean error = 242 m, SD = 144). The mean error estimate from these tests was used to constrain analyses of the spatial dataset, including the smoothing bandwidth of kernel density estimates (300-m) and grid cell size for spatial modelling (600-m).

Detection of porpoises

It is not possible to use Conventional Distance Sampling (CDS) methods on data collected in single point, land-based observation surveys, because of violation of the assumptions of Distance Sampling theory (Buckland et al., 2001). As a result, there is no way to estimate the effect of distance on the ability of observers to detect animals recorded in this survey using CDS methods. Instead, a series of independent double-observer trials were carried out at the

same site using a surveyor's theodolite, and the results were modelled in a logistic regression in order to estimate a detection function (Nichols et al., 2000; Buckland et al., 2008). The detection function was then used to systematically correct for the proportion of missed animals with increasing distance (Buckland et al., 2004).

The double-observer trials were undertaken retrospectively, during 2012 and 2013, in an attempt to better constrain the impact of detection bias on the results of the monitoring survey carried out in previous years (2007–2010). Although the trials were collected at a different time to the original survey data, the overall survey conditions and observer experience were comparable; therefore it is deemed valid to use the resulting detection function to correct the dataset that was previously collected at the site (personal communication: Dr. Len Thomas, Centre for Research into Ecological and Environmental Modelling). If both of the observers independently detected the same animal(s), the trial was recorded as successful; if only one observer detected the animal(s), the trial was a failure (detailed methods are provided in Section S1.1. of the Supplementary Material). 16 double observer trials on porpoise sightings were carried out during the limited data collection period at the survey site in 2012–13. Although the sample size is acknowledged to be small, in the absence of a more powerful dataset, the trials data were modelled using a logistic regression to estimate the probability of detection as a function of distance from the observer. The standard Distance Sampling assumption of $g(0) = 1$ was used, i.e. the probability of detection at a distance of 0 km from the observer equals 1 (Buckland et al., 2001), and the model-estimated detection function is presented in Fig. S1 of the Supplementary Material. The detection function was used to predict the probability of detection within each grid cell, based on the distance of the grid cell centre from the observer's position.

The sightings within each grid cell were then corrected using the model-predicted detection probabilities. The detection-corrected data were supplied as the response variable in the subsequent model of the spatial distribution of porpoises within the survey area.

Because of the low sample size for the double observer trials, additional measures were also used to ensure the visual survey methods had not been affected by bias related to detectability, and to support the robustness of the dataset and analyses. These included analysis of (1) distance distribution data for other species recorded during visual surveys, and (2) an additional boat-based survey dataset collected within the survey area (details of these analyses are provided in Sections S1.2. and S1.3. of the Supplementary Material). The boat-based data showed a similar spatial pattern in relative density of porpoise sightings as the land-based survey data; therefore we are confident that detection bias did not significantly affect the observed spatial distribution pattern of porpoise sightings (Supplementary Material, Figs. S3 and S4). On the basis of the outcome of these investigations, the effective survey area was delineated at a distance of 3 km from the survey watchpoint on Gwennap Head (Fig. 1).

Data analysis

Harbour porpoise sightings data treatment

Data filters were applied to the 4020 h of total survey effort (containing a total of 736 porpoise sightings) in order to remove effort and sightings recorded during poor survey conditions, defined as visibility <5 km and/or Beaufort sea-state of >3. Sightings recorded outside of the delineated survey area (100–270° and out to 3 km) were also removed, as were known or suspected re-sightings of the same individuals or groups. The final filtered-sightings dataset contained 2413 h of survey effort, and 418 sightings of harbour porpoise (Table 1). All sighting records retained in the dataset had associated distance estimates (in order to ensure they were within the delineated survey area), but only those sightings that also had precise bearings recorded (as opposed to cardinal directions) were used in the spatial analyses. The spatial dataset contained 255 sighting records.

The visually estimated locations of the filtered spatial sightings dataset ($N = 255$) were transformed from bearing and distance to decimal degree coordinates (Veness, 2012) and imported into a GIS where they were mapped over the high-resolution bathymetry map. Mapping was carried out in ArcGIS v.10 and all statistical analyses were performed using the R software (R Development Core Team, 2011).

Cluster analysis

The spatial distribution of porpoise sightings within the survey area (un-corrected for detection bias) was explored using a Ripley's *K* analysis in the R package 'spatstat' (function 'kest', Baddeley and Turner, 2005). The test is a second order analysis of spatial point processes that examines the distribution of distances between

points over various scales to look for scale-dependent patterns. The cluster statistic, $K(d)$, represents the intensity of points within specified distances bands (d) from other points, and is compared to an expected K value based on 999 simulations of complete spatial randomness.

Kernel density

Utility distributions (UD) (Powell, 2000), describing the pattern of porpoise sighting intensity in the raw sightings data (uncorrected for detection bias) within the survey area, were estimated using un-weighted fixed kernel density estimation (KDE) and kernel isopleths, calculated in the Geospatial Modelling Environment software (Beyer, 2012). The X and Y coordinate data for the porpoise sightings were normally distributed; therefore a quartic approximation of the Gaussian kernel was used, which gives a uni-modal kernel that is symmetrical around the origin (the estimated sighting position).

Bandwidth (h) optimisation was carried out using functions in the R package 'sm' (Bowman and Azzalini, 2010). Selection of h was based on visual comparison of performance and minimisation of the mean square error. A value of $h = 300$ m (estimated using an un-weighted normal smoothing method) was used in the kernel density estimate calculations. Powell (2000) recommends using a smoothing bandwidth that is at least equal to the uncertainty in the location estimates, therefore the selected value of 300 m is appropriate considering the error on the sighting position estimates. The 50% KDE isopleth was selected to define a core-use area within the survey area; on the basis that this will delineate the area of 50% probability of sightings, which contains approximately 50% of the observations (Börger et al., 2006).

Generalised Additive Modelling (GAM) methods

Generalised additive models (GAMs), with Poisson or negative binomial error structure (dependent on presence of overdispersion), were used to model spatial and temporal patterns in the porpoise sighting data. The GAMs take the general structure specified by Hastie and Tibshirani (1990) and were carried out in the R package 'mgcv' (function 'gam', Wood, 2006), which contains integrated smoothness estimation. Smooth functions for model covariates were specified using thin plate regression splines with shrinkage (Wood, 2006). For most model covariates, the dimension, k, representing maximum degrees of freedom of each smooth, was manually limited by $k = 4$ to avoid excessive flexibility and model over-fitting. The smoother of time to high water (TtHW) in the temporal model was given maximum $k = 6$, to allow for the expected sinusoidal patterns in sightings with respect to tide. The penalty (*gamma*), given to each degree of freedom in the automatic smoothing parameter selection process, was increased from the default of 1 to 1.4, as recommended by Wood (2006) to reduce the potential for model over-fitting. Interactions between covariates were modelled using tensor product (te) smooths. Aspect and TtHW were modelled with cyclic smoothers to account for the circular nature of the degree unit of aspect (where 0 and 359

Table 1
Summary of survey effort and harbour porpoise sightings from the visual monitoring survey, 2007–2010 (after filtering for poor survey conditions and quality control). 'Positive' hours/days are defined as periods during which one or more porpoises were recorded.

Year	Hrs obs	Sightings	% Positive hrs	% Positive days	% Survey effort by Beaufort sea state (% sightings)			
					0	1	2	3
2007	608	86	11.35	35	3 (12)	21 (12)	46 (59)	30 (17)
2008	538	124	16.54	34	2 (5)	17 (46)	41 (25)	40 (24)
2009	569	128	18.10	42	2 (4)	25 (54)	45 (28)	28 (14)
2010	698	81	9.17	33	1 (2)	19 (41)	47 (51)	33 (6)
All Years	2413	419	13.47	36	2 (6)	20 (40)	45 (38)	33 (16)

Table 2
Names and definitions of all explanatory variables used in the analyses of spatial and temporal patterns in the distribution of porpoise sightings.

Variable	Model	Description of variable
Av. Depth	Spatial	The average depth value for each grid cell, calculated from the mosaic of 1 m and 12 m resolution bathymetry data. Measured in metres below the surface
Av. Slope	Spatial	Slope of the seabed, derived from the bathymetry data using using the maximum change in elevation of each of the bathymetry layer cells and its 8 neighbours (i.e. a 3 × 3 cell window). The value used in the model was the average slope value (gradient in degrees) for each of the survey area grid cells
Av. Aspect	Spatial	Aspect was derived from the bathymetry data and identifies the downslope direction of maximum rate of change in value from each of the bathymetry layer cells and its 8 neighbours (i.e. a 3 × 3 cell window). This metric can be thought of as the direction of the slope, and is measured in clockwise degrees from 0 (due north). Flat areas are given a value of −1. The value used in the model was the average aspect value for each of the survey area grid cells
Slope:Aspect	Spatial	The interaction term between the slope and aspect covariates for each grid cell
Depth:Slope	Spatial	The interaction term between the depth and slope covariates for each grid cell
Depth:Aspect	Spatial	The interaction term between the depth and aspect covariates for each grid cell
Year	Temporal	Year of the survey. Factor variable with 4 levels (2007, 2008, 2009, 2010)
Month	Temporal	Month of the survey. Factor variable with 4 levels (July, August, September, October)
Beaufort sea state	Temporal	From the hourly observations of survey conditions collected by observers at the watchpoint, using the Beaufort scale. Factor variable with 4 levels (0, 1, 2, 3)
TtHW	Temporal	Time to high water. In decimal hours relative to HW time, where HW = 0. Values range from −6.33 to +6.33. Calculated using HW times from the POLPRED CS20 model for location within survey area (Proctor, Bell et al., 2004)

are adjacent values) and the cyclic nature of the tidal cycle (+6.3 to −6.3 h relative to HW time).

Retention of collinear variables in a model can lead to poor estimation of standard errors and p-values. To avoid the problems introduced by correlation between covariates, pairwise Spearman's rank correlation tests and Variance Inflation Factors (VIF) (R 'AED' package, function 'corvif', Zuur et al., 2009) were calculated for all of the candidate model covariates. Pairs of variables with high levels of correlation (Rho = ⩾0.6) or VIF values exceeding the conservative threshold of 3 (Zuur et al., 2009) were identified. For collinear pairs, the covariate that was selected first during the stepwise selection process was retained, while the other was discarded.

Predictor variables were selected through manual stepwise forwards selection, using the model fit score (AIC) to select the best model at each step. At each step, the significant ($p < 0.05$) covariate that added most explanatory power (⩾1% increase on previous model iterations) and resulted in the lowest AIC was selected. The AIC score must have been reduced by a value of 2 or more for a covariate to be considered for addition to the model (Burnham and Andersen, 2002). The updated model was then taken forward into the next round of selection, where the effect of adding the remaining predictor variables was tested again using the same method; and so on until no more covariates could be added, according to the above criteria.

Gridded relative density analysis

A radial grid was defined by the extent of the survey area (100–270° out to a distance of 3 km from the observer's location on Gwennap Head) and divided into cells along concentric distance bands from the watchpoint location at 600-m intervals, and radial bearing lines at 10° intervals (representing ± the mean error on visual position estimates, see Section 'Estimating error in sighting position estimates'). Number of porpoise sightings and area (km²) were calculated for each grid cell, along with associated values for mean depth, slope and aspect in each cell.

The detection function, created using a logistic regression on binary data from independent double observer trials collected at the survey site in 2012/13, was used to correct the data for missed sightings. For further information on the double observer trials and modelling methods see Sections 'Detection of porpoises' and S1.1. The sightings recorded within each grid cell were then corrected for detection using:

$$D_{sightings(i)} = N_{sightings(i)}/P_{(i)}$$

where $D_{sightings(i)}$ is the detection corrected sighting density in the ith grid cell, $N_{sightings(i)}$ is the number of sightings observed within the ith grid cell, and P is the modelled detection probability for the distance from the observer to the centre of the ith grid cell.

The detection-corrected counts of porpoise sightings per grid cell were then modelled as a function of static physical covariates within a Generalised Additive Model (GAM) framework. Models had a negative binomial error distribution (to account for overdispersion) and all candidate covariates are presented in Table 2. The models included an offset of (logged) grid cell area, to account for differences in the area of the radial grid cells.

Standard model validation was carried out (as outlined by Wood, 2006; and Zuur et al., 2007), and spatial autocorrelation was checked using the residuals from the final model in a Mantel test (R package 'Vegan', Oksanen et al., 2013). The test calculates Pearson correlations from dissimilarity matrices of (1) the distance between pairs of points (locations of grid cell centroids) and (2) the differences in model residual values between pairs of points. The calculated correlation of the modelled data is then compared to correlation calculated on 999 random reassignments of residual values to location points (retaining the spatial structure of the data, Legendre and Legendre, 2012).

Effect of tidal flow on the temporal distribution of porpoise sightings

The number of porpoise sightings per hour was modelled using a GAM with Poisson error distribution and log-link. Candidate model covariates are listed in Table 2. Standard GAM validation was carried out, and an assessment of dependence structure in the residuals of the final model was undertaken using an autocorrelation function ('acf') in R.

Oceanographic survey

A fine-scale ADCP survey was undertaken within the survey area over a semi-diurnal tidal cycle on 11th July 2011 (2 days after neap tide). The aim of the survey was to identify flow features, driven by the interaction with topography, which may be relevant in the context of fine-scale harbour porpoise distribution. The survey was carried out aboard the University of Southampton inshore vessel, *RV Callista*, using a hull-mounted RDI Workhorse Mariner in bottom tracking mode. The ADCP frequency was 600 kHz and ping rate was 2 Hz (2 cycles per second). Vertical bin size was 1-m and ensemble interval was set at 2 s (4 pings per ensemble). The ADCP transect route (Fig. 1) was repeated nine times over a 12.6 h tidal cycle. The vessel's average speed of travel throughout the survey
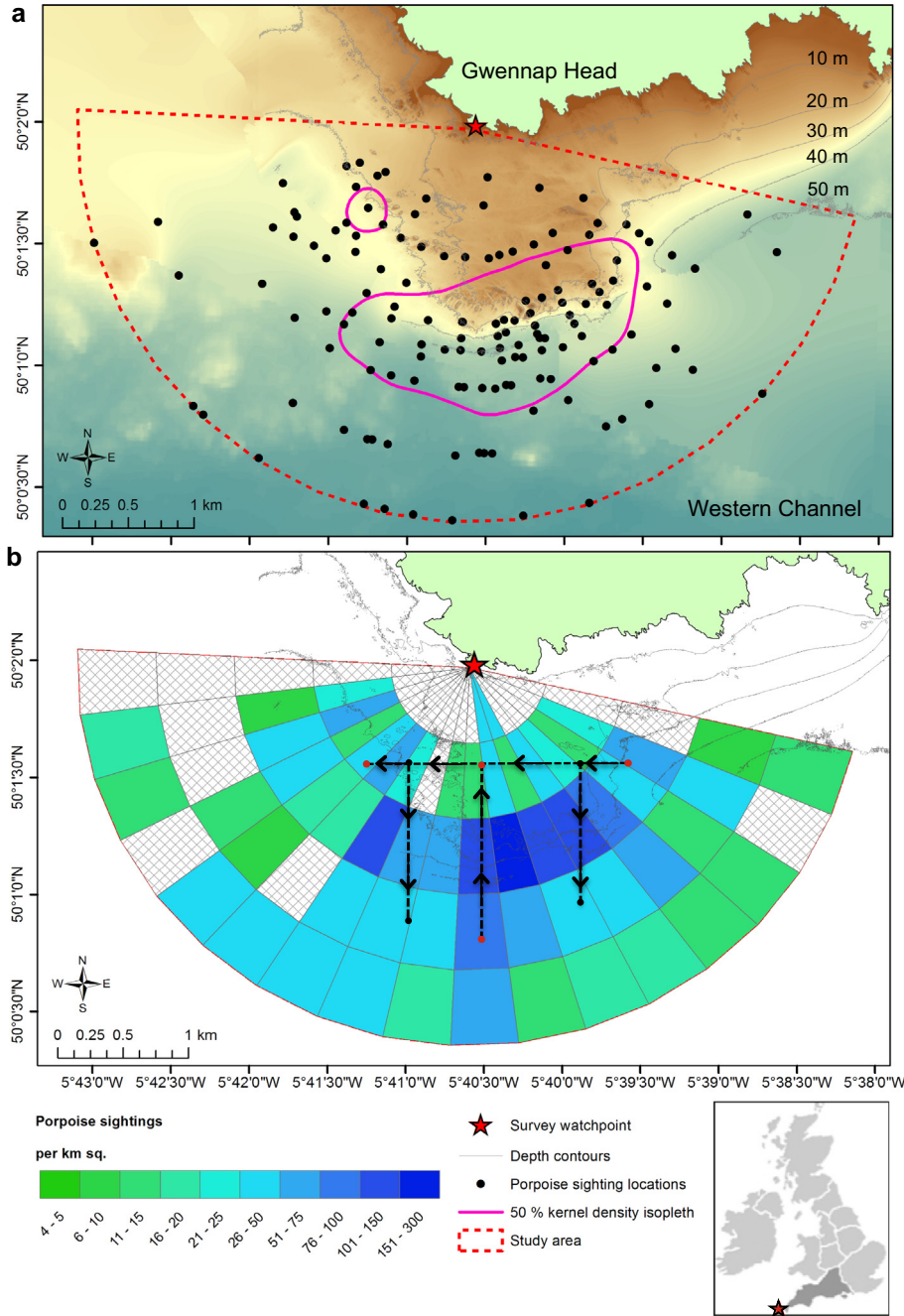
Fig. 2. (a) Raw data: filtered harbour porpoise sightings (N = 255) and 50% kernel density estimate isopleth (smoothing bandwidth = 300 m). (b) Detection-corrected porpoise sighting density by grid cell (N = 85), corrected for cell area and presented as sightings per km². Hatched cells contained 0 sightings. Reef contours (10 m intervals) are shown. Oceanographic survey transect route is overlain (for detailed transect route map see Fig. 1).

was 5.14 knots, and average sea state was Beaufort 1.5 (SD = 0.5). Vertical shear, S, in the horizontal velocity across 1-m vertical intervals was calculated as:

$$S = \left((\partial U/\partial z)^2 + (\partial V/\partial z)^2\right)^{1/2}$$

where $\partial U/\partial z$, $\partial V/\partial z$ are the vertical gradients in the east and north velocity components, respectively. Shear was computed over 1-min intervals (average of 30 × 2-s ensembles).

Conductivity Temperature Depth (CTD) and fluorescence data were collected throughout the ADCP survey at waypoints (WP) 1, 2, 5, and 6 (Fig. 1) using an FSI CTD with fluorometer, mounted on a 12-bottle CTD rosette. Data were processed using FSIpost

and have been used to investigate patterns in density and fluorescence through the tidal cycle at key sample sites and to calculate a Richardson Number depth profile during tidal periods associated with high and low porpoise sightings. The Richardson number (Ri) indicates the susceptibility of a stratified fluid to the generation of turbulence by shear-instability. Ri, computed over 1-m vertical intervals, was calculated as:

$$Ri = N^2/S^2$$

where $N = (-g/\rho_o \partial \rho/\partial z)^{1/2}$ is the buoyancy frequency and dependent on the vertical density gradient, $\partial \rho/\partial z$. Ri < 0.25 is indicative of transition from laminar to turbulent flow (Miles, 1961). An estimate of Ri was calculated using data from, firstly, WP5 because this was the

Table 3
Summary of negative binomial GAM of detection-corrected porpoise sightings per grid cell (N = 85 cells). See Table 2 for description of variables and full list of candidate covariates that were considered during model selection. Variables are shown in the order of selection, with terms being selected sequentially based on reduction in AIC score compared to the previous model (with the starting AIC score given in bold in top row) and the amount of deviance explained by each term addition. All selected terms were significant to at least $p = 0.05$. The degrees of freedom of the estimated smooth functions are given as 'edf'.

Order	Linear term/smooth (df)	% Deviance	Adjusted R	AIC	Chisq.	Estimated p-value
Null	**Intercept = 3.36**	**0**	0.1	**381.9**		
1	S(average slope), edf = 1.1	17.8	0.4	397.4	9.5	<0.001
2	S(average depth), edf = 1.1	13.8	0.5	382.1	47.1	<0.001
3	S(average depth: average aspect), edf = 8.2	14.9	0.5	379.8	16.0	0.024
Final	*S(average depth) + S(average slope) + S(average depth: average aspect)*	*46.5*	*0.5*	*379.8*		

Dispersion (sum(resid^2)/residual degrees of freedom) = 1.02.
Total model degrees of freedom = 11.47.
K = 2.919.

## Results

Harbour porpoise survey

Harbour porpoises were sighted on 135 of the 372 survey days between 15th July and 15th Oct 2007–2010. The highest rate of sightings was recorded in 2009 and the lowest in 2010 (Table 1). Group sizes of up to 20 porpoises were recorded, though single animals were most frequently observed (41%). The average pod size per sighting was 2.33 animals (SD = 2.02). The proportion of survey effort during each sea state (0–3) was similar throughout all four years of the survey (Table 1); therefore it is unlikely that changes in survey effort with relation to sea state would account for the inter-annual variability in the recorded numbers of sightings.

Sea state conditions had a considerable effect on the number of harbour porpoise sightings recorded per hour. As sea state increased, there was a corresponding decrease in the rate of sightings per hour of effort; therefore sea state was included as a covariate in the model of the temporal distribution of porpoise sightings (see Section 'Fine-scale temporal distribution of porpoise sightings in relation to temporal variables'). The highest sighting rate was 0.48 porpoises per hour in sea state 0, although this sea state was very rarely observed (Table 1). The sighting rate reduced to 0.38 in sea state 1 and 0.15 in sea state 2. During sea state 3, the sighting rate was only 0.08, which represents a 6-fold decrease compared to the rate in sea state 0.

A two-sample Kolmogorov–Smirnoff test was carried out on pairwise comparisons of the density distribution of porpoise sightings by distance from observer, under each sea state (0–3). Although sea state was shown to clearly affect sighting rate at the study site, the comparison of the spatial distribution of sightings showed no significant difference in the density-by-distance curves in all pairwise tests ($p = >0.08$, with correction for multiple testing, see Fig. S5 and Table S1 in Supplementary Material Section S2). This suggests no systematic bias caused by sea state on the observed spatial distribution of sightings.

Spatial clustering of porpoise sightings

Porpoise sighting locations (N = 225), uncorrected for detection, are shown in Fig. 2a. Results of Ripley's K analysis showed that porpoise sightings were significantly clustered ($p = <0.001$, N = 255 sighting locations). The 50% UD kernel isopleth (N = 255 sighting locations) had an area of 1.87 km^2, representing just 14% of the full survey area of 13.3 km^2, but containing approximately 50% of
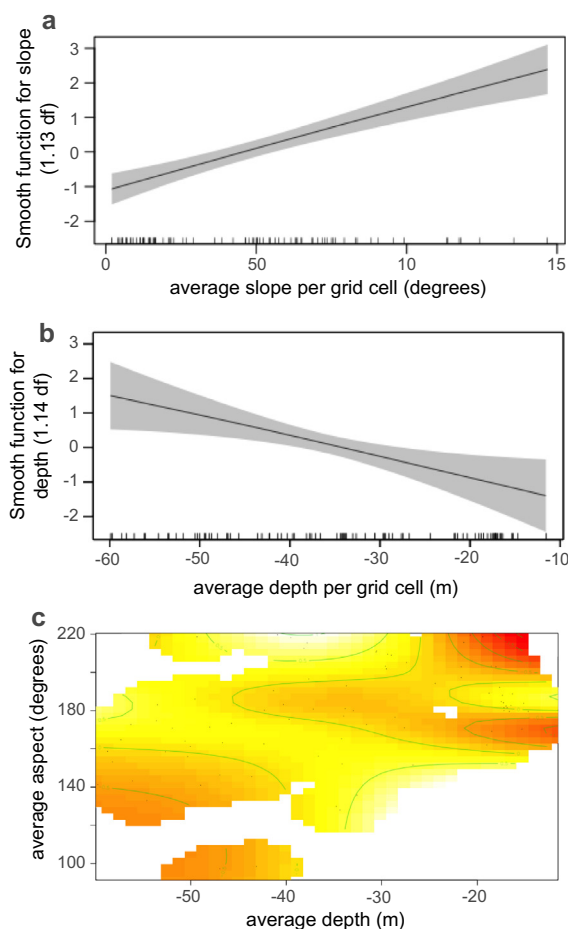
Fig. 3. Spatial distribution of harbour porpoise sightings modelled using a GAM with negative binomial error structure. (a) Smooth function of average slope within grid cells and (b) Smooth function of average depth within grid cells. Shaded areas represent 95% CIs and rug plot along *x* axis shows observed data values. (c) Heat plot with overlaid contours for the smooth interaction term of depth and aspect within each grid cell. Strength of interaction effect is colour scaled, with warmer colours indicating combinations of depth and aspect with greatest effect on porpoise sightings. (For interpretation of the references to colour in this figure legend, the reader is referred to the web version of this article.)

porpoise sightings. The position of the 50% UD isopleth indicates that clustering of porpoise sightings occurs around the southern and south-eastern margins of the Runnelstone Reef (Fig. 2a). There was no notable change in the location of the 50% isopleth when kernels were calculated for subsets of sighting locations collected in different years or under different flow conditions.

The survey area was divided into a total of 85 grid cells, 58 of which had at least one porpoise sighting recorded within them

Table 4
Summary of Poisson GAM of porpoise sightings per hour of survey effort (N = 4019 h). See Table 2 for description of variables and full list of candidate covariates that were considered in model selection. Variables are shown in the order of selection, with terms being selected sequentially based on the reduction in AIC score compared to the previous model (with the starting AIC score in top row in bold) and the amount of deviance explained. All selected terms were significant to at least $p = 0.05$. Degrees of freedom for estimated smooth functions are given as 'edf'.

Order	Linear term/smooth (df)	% Deviance	Adjusted R	AIC	L (df)	Estimated p-value
Null	**Intercept = −1.75**	**0**	**0**	**2465.8**		
1	Beaufort sea state (factor with 4 levels)	7.9	0.04	2346.4	195 (3)	<0.001
2	Month (factor with 4 levels)	7.1	0.1	2213.9	137 (3)	<0.001
3	Year (factor with 4 levels)	2	0.12	2184.7	35 (3)	<0.001
4	Smooth (TtHW), edf = 3.5	2	0.13	2158.1	34 (3.5)	<0.001
Final	Month + Beaufort sea state + Year + s(TtHW)	**19**	**0.132**	**2158.1**		

Dispersion (sum(resid^2)/residual degrees of freedom) = 1.15.
Total model degrees of freedom = 13.49.

(Fig. 2b). Grid cells containing the highest numbers of detection-corrected porpoise sightings per km² were located in a radial band along the reef edge, between 1.2 and 1.8 km from the survey watchpoint location (Fig. 2b).

Spatial model of porpoise relative density

The best model of the detection-corrected porpoise sightings per grid cell explained 46.5% of the deviance in the fine-scale spatial distribution of harbour porpoise sightings as a function of the covariates slope, depth, and an interaction of depth and aspect (Table 3). Slope was the most significant predictor variable ($p = <0.001$), explaining 17.8% of the deviance, with depth and the interaction between depth and aspect explaining another 13.8% ($p = 0.01$) and 14.9% ($p = <0.001$) of the deviance respectively (Table 3). Porpoises were more frequently recorded within areas of high average slope and intermediate to high average depth (Fig. 3a and b). The interaction term indicates a preference for areas where shallow to moderate depth is combined with slopes of southerly and south-westerly aspect (Fig. 3c). These conditions predominate

around the southern Runnelstone Reef margins and the steep pinnacles. There was no spatial autocorrelation in the model residuals (Mantel statistic $r = −0.043$, significance based on 999 permutations = 0.175), which justifies the use of a GAM model structure that does not include an autocorrelation parameter to account for spatial dependence.
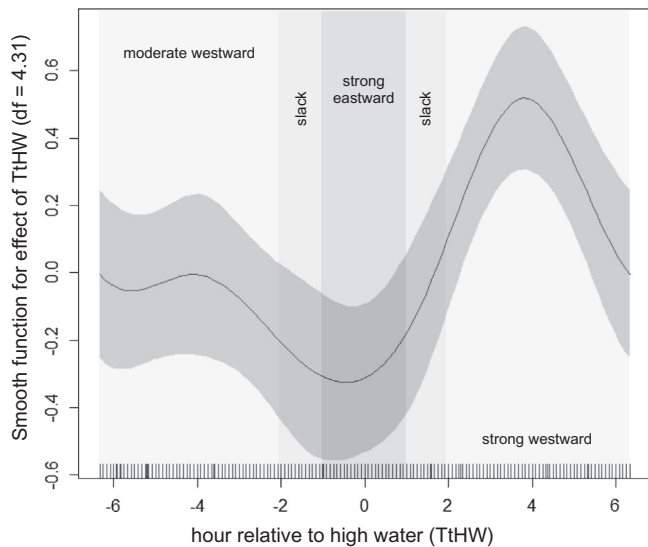
Fine-scale temporal distribution of porpoise sightings in relation to temporal variables

GAM analysis found the covariates TtHW, Beaufort sea state, year and month as significant explanatory variables; explaining 19% of the temporal variability in porpoise sightings (Table 4). Highest numbers of sightings were recorded in 2008 and 2009 (Fig. 4a). Sighting rates reduced as sea state increased (Fig. 4c) and there were higher sightings per hour recorded in July and October compared to August and September (Fig. 4b). Greater numbers of sightings were recorded during hours when the tide was flowing to the west (ebbing), particularly between 2 and 6 h after HW (Fig. 5), corresponding to the period of strongest west-
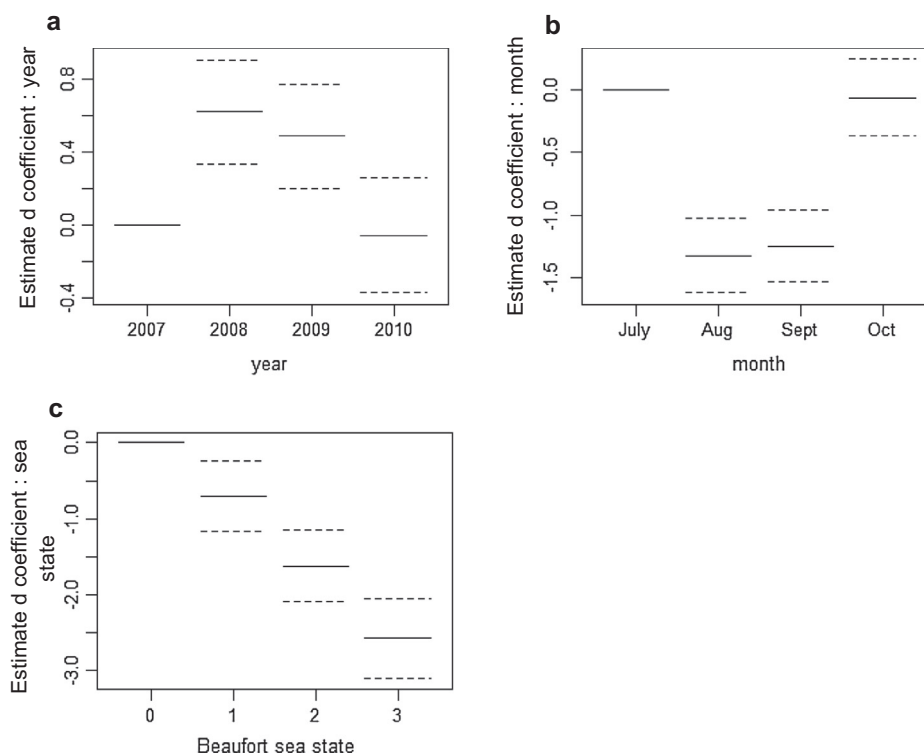
Fig. 4. Termplots showing estimated partial coefficients for parametric explanatory variables in the Poisson GAM of harbor porpoise sightings per hour: (a) year of survey, (b) month of survey, (c) Beaufort sea state. Base level of each factor variable is centered at 0.95% confidence intervals are shown by dashed lines.

Fig. 5. Harbour porpoise sightings temporal distribution modelled using a GAM with Poisson error structure: estimated smoother for the effect of time to high water (TtHW) on harbour porpoise sightings per hour. Shading around line indicates 95% confidence interval. Vertical shading bands on plot show predominant flow direction in the survey area during each hour of the tidal cycle. Rug plot of observed TtHW values is also shown.

ward flow. Much lower sighting rates were recorded between −2 and +1 h relative to HW, which are characterised by eastward flow and slack water periods (Fig. 5). The rug plot along the bottom of

Fig. 5 indicates all observed values of TtHW, showing a good spread of effort throughout the full tidal cycle. A non-parametric two-sample Kolmogorov–Smirnov test (2-sided) indicated significant differences in the temporal distribution of porpoise sightings with reference to tidal flow, when compared to the overall distribution of effort; indicating that the results are not simply a function of the distribution of survey effort ($D = 0.1161$, $p = $<0.001). There was no significant temporal correlation structure in the final model residuals, therefore no requirement to use a mixed model to account for temporal autocorrelation.

*Oceanographic survey*

Current and density fields

Images showing the ADCP data (flow velocity and shear) from a selection of periods throughout the surveyed tidal cycle are given in Figs. 6 and 7, with further ADCP transect data in the Supplementary Material (Figs. S6 and S7). The ADCP survey recorded relatively strong tidal flows at the site during the survey (up to 1 m s^{-1}), as well as complex fine-scale flow patterns and hydrodynamic features (Figs. 6 and 7, S6 and S7). Flow over the shallower reef top area was generally faster than in the deeper water at the reef edges and beyond (by between 0.2 and 0.6 m s^{-1}; Fig. S6a). Tidal asymmetry was apparent in the eastward velocity component, *U*; currents were directed to the east only during groups 5 and 6 and were otherwise directed to the west (Fig. 7a and b). Similarly the weaker northward current component, *V*, exhibited a brief reversal along leg 3 from northward to southward (Fig. 7a). A significant difference was apparent in *V* between legs 3 and 4, both of which were orientated north to south, as shown on the transect route
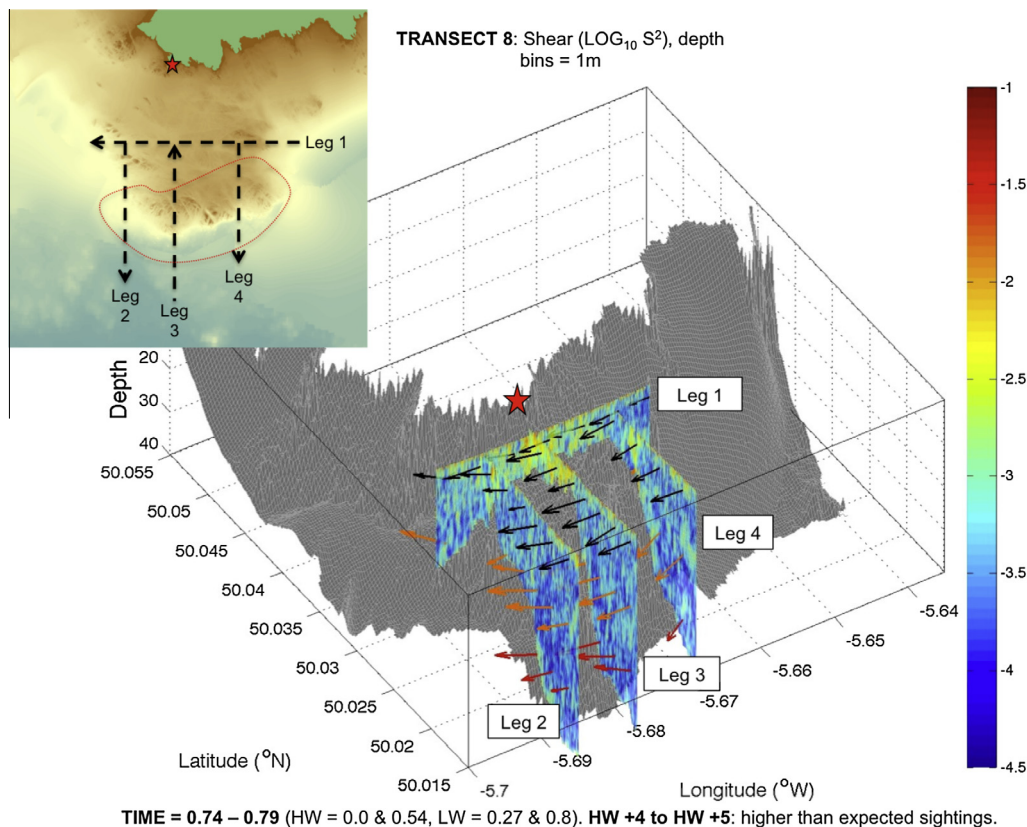
Fig. 6. Shear squared (log$_{10}$ S^2) computed over 1-m vertical intervals for the eighth transect run (approximately HW +4 to HW +5). Velocity vectors (indicated by arrows) are plotted at 90-s intervals along each leg at depths of 5 (black), 15 (orange) and 30 m (red). Current profile data were collected as 2-s ensembles in 1- m depth bins from a hull mounted ADCP on the *RV Callista*. Insert identifies transect line location with reference to the 50% UD of the visual porpoise sightings. Red star shows position of visual survey watchpoint on Gwennap Head and gray background is bathymetry. (For interpretation of the references to colour in this figure legend, the reader is referred to the web version of this article.)
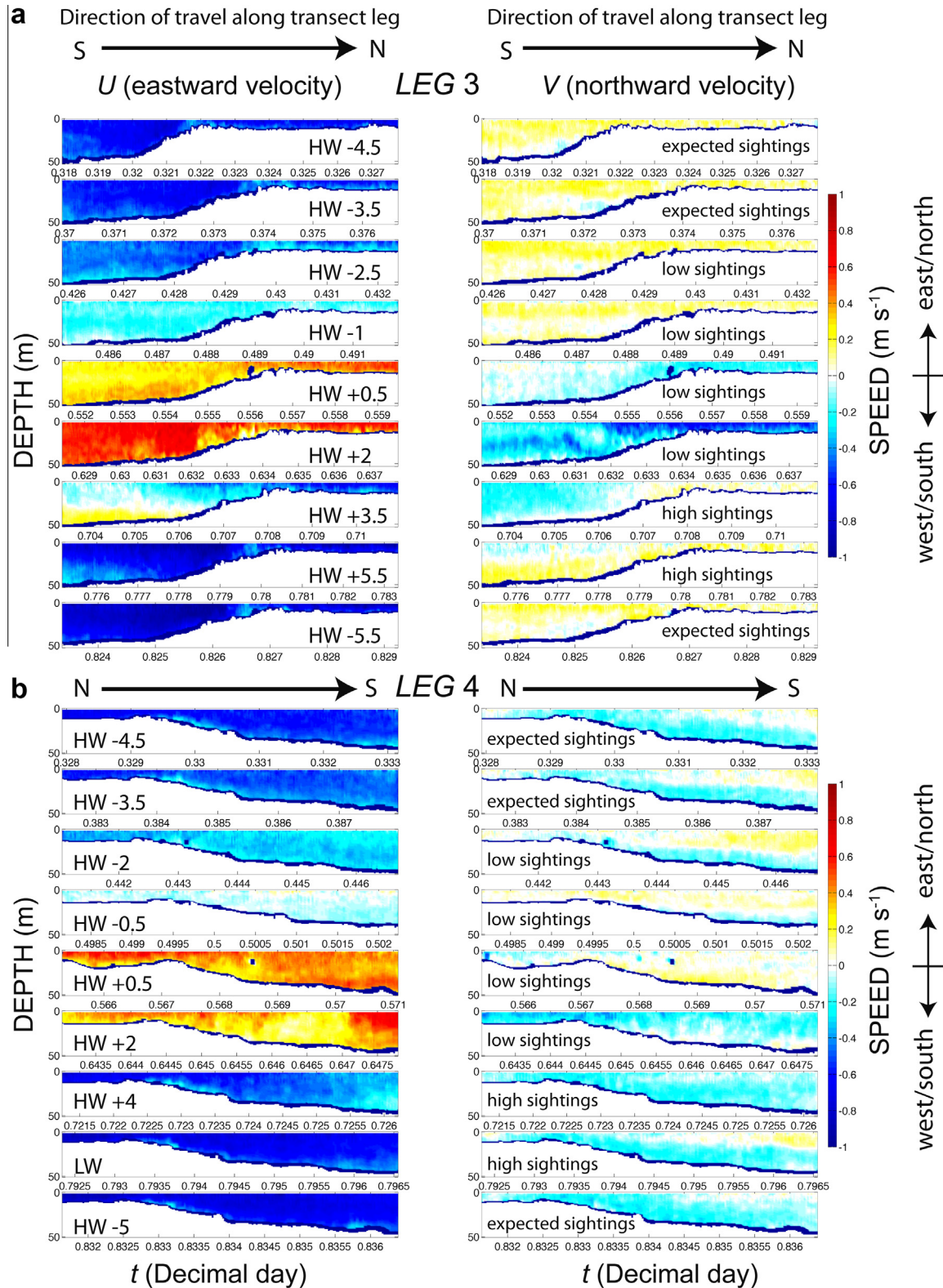
Fig. 7. Current velocity profiles from transect groups (G) 1–9 of the ADCP survey in the study area, carried out on 11th July 2011 from *RV Callista*: (a) leg 3 (travelling south to north) and (b) along leg 4 (travelling north to south) Data are from a full tidal cycle. Decimal time relative to HW (0 and 0.5) is given along the *x* axes and water depth along the *y* axes. Current velocity is colour scaled with (a) the eastward velocity component, from east in red to west in dark blue and (b) the northward velocity component, from north in red to south in dark blue. The timing of each profile relative to HW and to relative density of porpoise sightings is labelled. (For interpretation of the references to colour in this figure legend, the reader is referred to the web version of this article.)
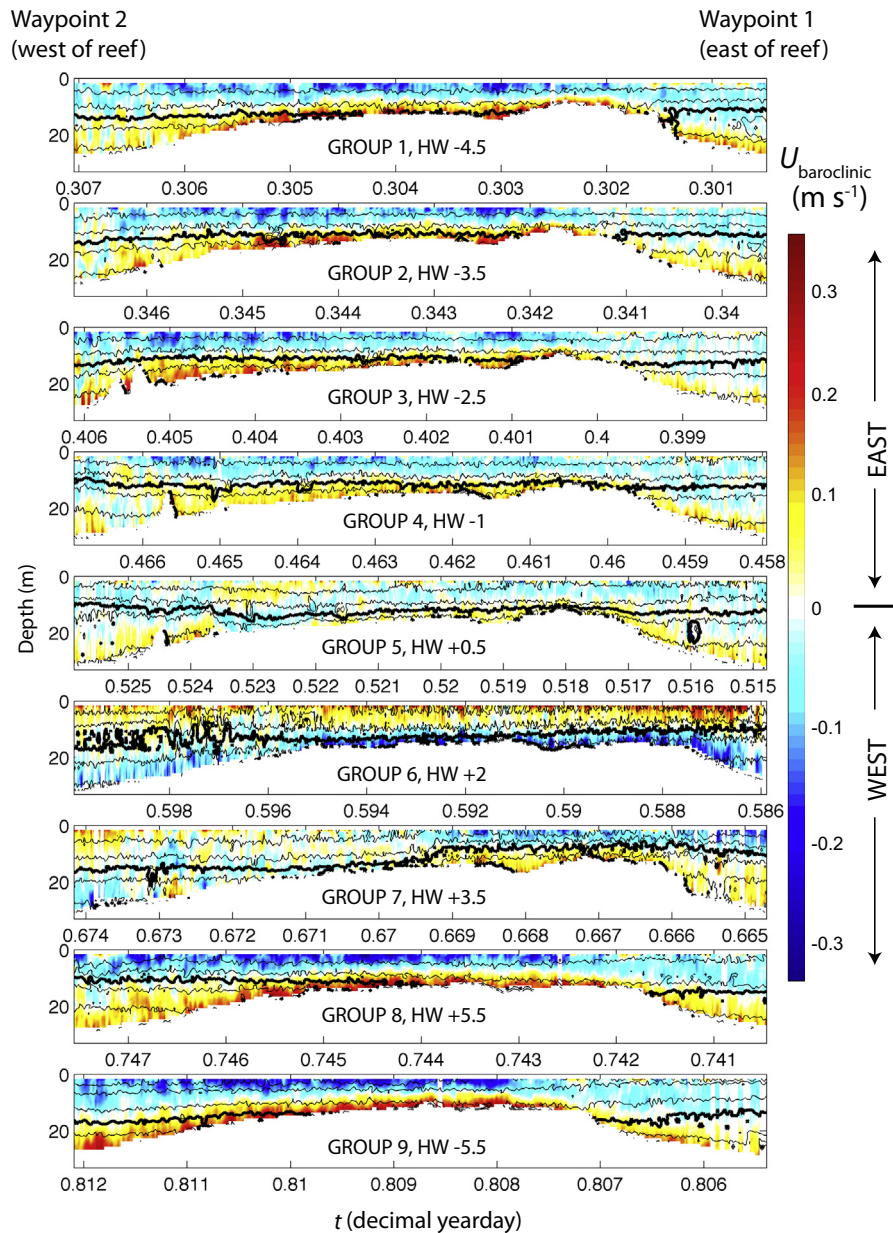
Fig. 8. Leg 1 baroclinic eastward velocities, $U_{baroclinic}$, computed as the total velocity following subtraction of the depth-mean component. Overlain are contours of echo intensity from the ADCP at 10 db intervals with the 110 db contour indicated by the heavy black line. The panels are reversed in time such that WP2 on the western side of the reef is on the left side of the figure; each leg began at WP1 and crossed the reef to WP2, i.e. from right to left when looking at the figure.

map in Fig. 1. Leg 3 was located centrally across the reef where depth contours started to turn northwards with respect to a westward flow. Leg 4 crossed the reef on its eastern edge where depth contours headed south for a current flowing in a westward direction. During leg 3, V was predominantly northward whereas within the same groups flow during leg 4 was predominantly southward (Fig. 7). Thus, flow followed depth contours around the outer flank of the reef and indicates a pronounced curvature in the velocity field in response to local bathymetry, as depicted by the velocity vectors in Fig. 6.

The flow is two-layered, manifested by flow reversal over depth in U during leg 3 around HW +3.5 (Fig. 7a), and exhibits a significant baroclinic component, estimated as the observed current following subtraction of the depth-mean barotropic component (Fig. 8). At times, these two-layered flows were associated with the formation of a mid-depth layer of elevated shear at a height

above bed (HAB) of ~25 m, within which $S^2 > 10^{-4}\,s^{-2}$. This shear layer can be seen along legs 3 and 4 during the period HW +4 to HW +5 as a mid-depth layer of lighter blue/green in Fig. 6. Two-layered flows were also observed during the westward ebbing tide in the northward velocity component along leg 4 from HW −4.5 to HW −2 and again at LW (Fig 7b).

The CTD and fluorescence data collected through the tidal cycle at four of the waypoints indicate that there was also a tidal asymmetry in water properties. The overall pattern is represented in Fig 9 by the data from waypoint 5 on the outer edge of the reef at the end of leg 3 (see location in Fig. 1). Fig. 9a shows that a body of warmer (less dense) surface water was advected along the coast through the end of the westwards ebbing tide (HW −3.5 to HW +0.5) and the period of the eastward flooding tide (HW +0.5 to HW +2). Cooler water was then flushed back through the survey site as the tide turned westward again (after HW +2) and through-
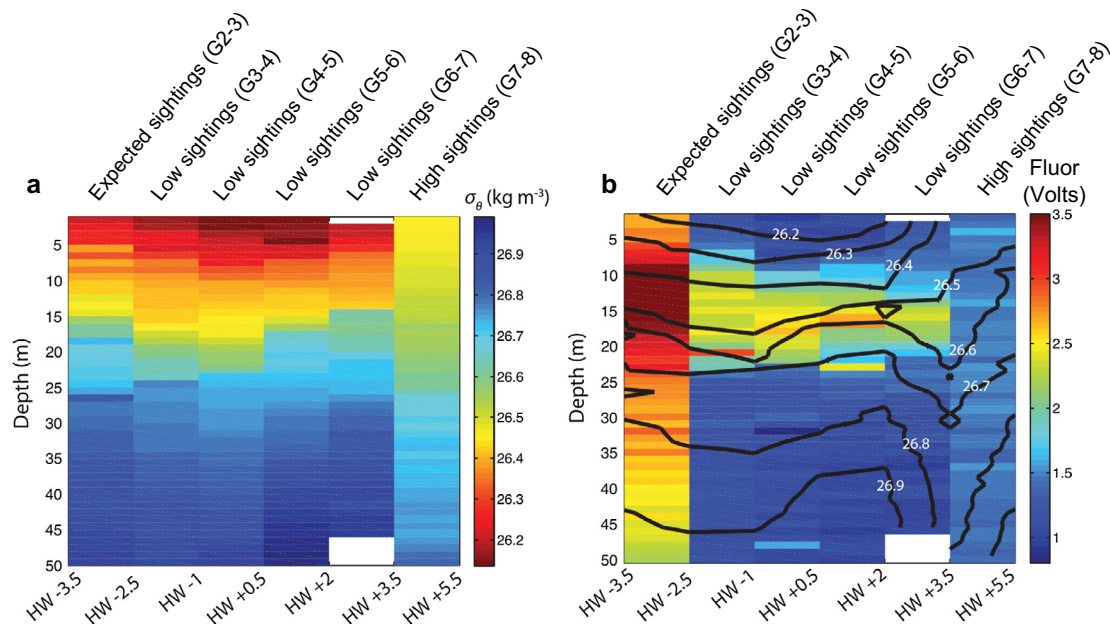
Fig. 9. (a) Density (σ_θ) and (b) fluorescence obtained from CTD casts at Waypoint 5 between transect groups 2 and 8. Labels at top relate to modelled porpoise sightings and are consistent with those in Fig. 7a, as are the times relative to HW. Fluorescence is indicated as Volts and overlain with isopycnals. Changes in density were due almost entirely to temperature, which decreased at the surface from a maximum of 15C at HW +0.5 to a minimum of 13 at HW +5.5.

out the following period of westward dominated current flow during transect groups 7–8 (HW +3 to HW −5.5). A mid-depth peak in fluorescence also occurred during the ebbing westward tidal flow and the following eastward flood between HW −3.5 to HW +3.5 (Fig. 9b); although this result is only representative of the sampling period and may not be consistent across all tidal cycles at the site. The overall pattern in the CTD data, from all four waypoints, showed cooler water and less thermal structure throughout the Runnelstone Reef survey during the westward ebbing tide (between HW +3 and HW −1); suggesting that regional-scale variations in water properties are advected past the reef during different phases of the tide (note the full CTD dataset from the entire survey area is not presented).

Internal shear and boundary layer turbulence

The pronounced vertical shear in the currents and the accompanying stratification (Figs. 6 and 7) suggest that shear-instabilities may play a role in promoting the development of turbulence throughout the water column. In the absence of direct measurements of turbulence, we firstly consider ADCP echo intensity as an indication of suspended material within the water column or stratified turbulence (van Haren, 2009). Echo intensity |E| varied strongly throughout the 12 h of observation but also with position relative to the reef (Fig. 10). During leg 4, which was the leg furthest to the east, |E| reached maximum values at each depth during groups 8 and 9 (Fig. 10) when the 110db contour (arbitrarily selected for indicative purposes) descended below the reef crest (Fig. 10). At this time currents had reversed from eastward to westward (Fig. 7a) and we propose that this deepening of 110db contour during the westward flow (Fig. 10, G8 and 9) indicates an increase in turbulence through shear instabilities attributable to the release of a lee wave generated during the eastward flood tide (G5 and 6); this is discussed in Section 'Internal lee waves and hydraulic jumps' with specific reference to the observed deepening of isopycnals on either side of the reef.

Further evidence for the role played by shear in promoting turbulence is found in the ADCP echo intensity data collected along leg 4 shown in Fig. 10. At *t* = 0.7955 (G8, HW +5.5), 5 cusps

extended downwards from the near surface layer (highlighted by black box in Fig. 10, G8) as the upper layer was flowing to the northwest, corresponding to an upstream but on-slope direction. The cusps closely resemble the form of Kelvin Helmholtz billows observed in oceanic conditions (van Haren and Gostiaux, 2010), and are strongly suggestive of shear-induced instabilities at moderate depths (~30 m).

To assess the likelihood that shear was elevated to the level required for shear instability in the region of highest sightings and the formation of the observed billows, we computed the Richardson number at adjacent WP5 (Fig. 11). Lowest values of *Ri* were observed at the times of highest porpoise sighting rates; during groups 7 and 8 (indicated by bold lines in Fig. 11). During group 7 critical *Ri* (<0.25) occurred in the lower half of the water column (below ~30 m) and the top half was only marginally stable (0.25 < *Ri* < 1). Conversely, the following group (G8) exhibited critical conditions indicative of shear instability and the generation of turbulence in the top half of the water column (above ~30 m), and marginally stable conditions below (Fig. 11), corresponding well with the depth where the billows were formed (~30 m depth, Fig. 10 G8). Importantly, during the tidal periods associated with reduced rates of porpoise sightings (G2–G6), *Ri* was significantly higher at WP 5 (Fig. 11); indicating a greater degree of stability and the reduced likelihood of shear-driven turbulence being generated in the core sightings area during these periods.

In addition to the generation of turbulence by shear instabilities in a two-layered flow (as observed in the ADCP data), frictional effects near the bed can also promote shear and turbulence. Analysis of the physics suggests that, for the maximum observed velocity of $O(1 \text{ m s}^{-1})$ recorded at HW +5.5, the corresponding Bottom Boundary Layer (BBL) would extend to HAB ~9 m (based on the calculation for height of BBL in a tidal flow proposed by (Lueck and Lu, 1997)). This provides evidence that the mid-depth shear layer evident along legs 3 and 4 between HW +4 and HW +5 (G7 and 8 in Fig. 7) at ~25 m HAB is not associated with frictional effects at the bed leading to an increase in the thickness of the BBL; but instead results from the baroclinic flow (Fig. 8, G7 and 8) and potentially the influence of topographic steering of flow
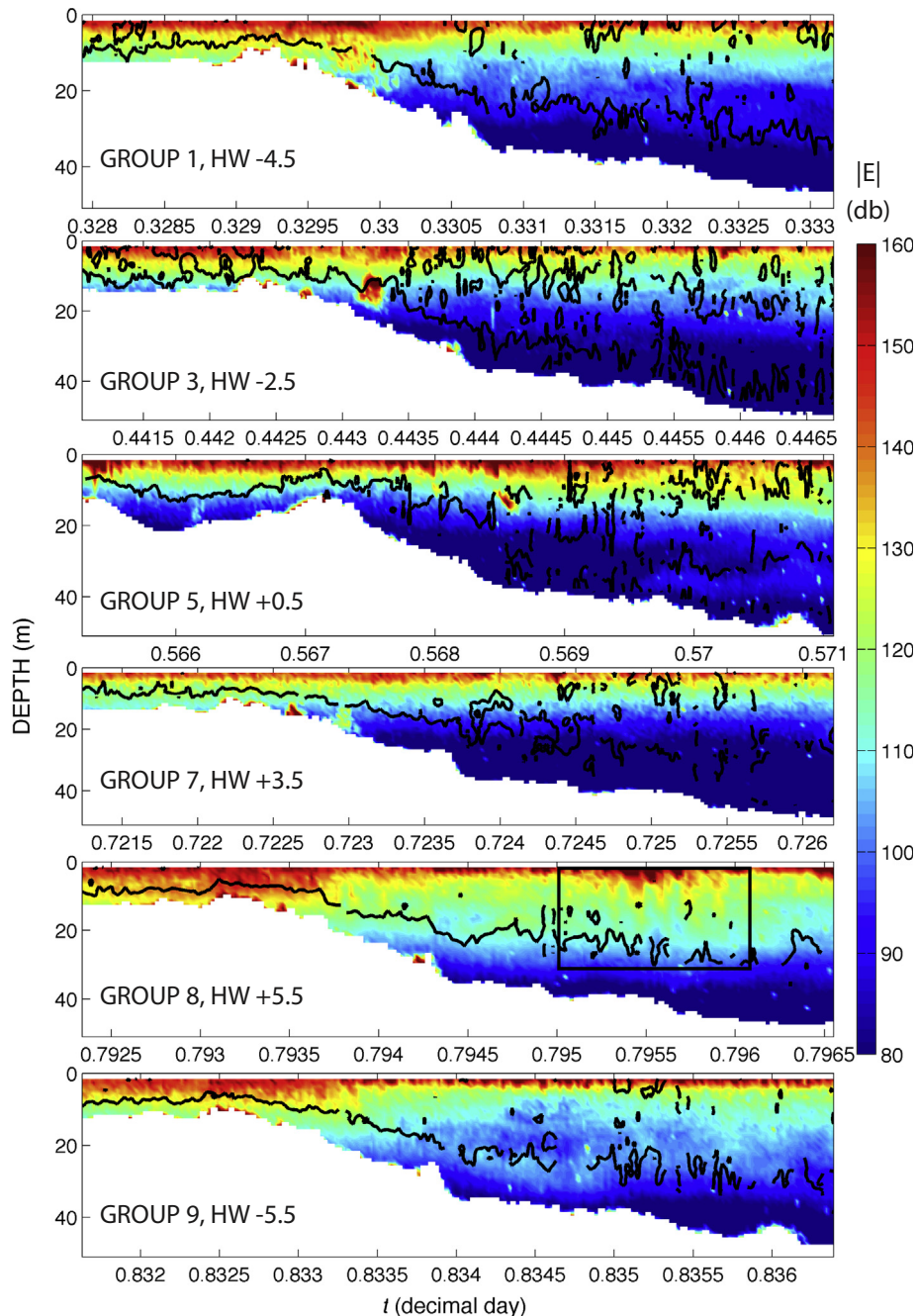
Fig. 10. Echo intensity |E| (db) during leg 4, which started on the reef and progressed offshore. The $U_{baroclinic} = 0$ contour is overlain on each panel. The black box in the profile for transect group 8 highlights the Kelvin Helmholtz instabilities that are strongly suggestive of shear-induced instabilities. Higher values of |E| indicate stronger turbulence and/or resuspended material. As the increase in |E| is clearly related to surface and interior processes rather than bed-processes, we consider that in this location |E| acts as a proxy for stratified turbulence.

around the reef (see velocity vectors in Fig. 6) and the larger scale hydrographic structure.

*Internal lee waves and hydraulic jumps*

Fig. 7 demonstrates that the primary flow direction at Runnelstone Reef was east/west, perpendicular to the subsurface ridge, suggesting that some of the water encountering the reef is forced over, rather than around, the reef. Lee waves can be formed under such circumstances, as the flow is forced over topographic irregularities (Geyer, 1993; Nash and Moum, 2001; Roughan et al., 2005). Despite the three-dimensionality of the Runnelstone Reef bank, a continuously stratified flow will pass over a gently varying

two-dimensional bottom as long as the height of the reef (~25 m) is less than U/N, where U is the free stream velocity and N is a representative buoyancy frequency (Hunt and Snyder, 1980). Here $U = 0.5$ m s^{-1} and $N = 0.01$ s^{-1}, such that $U/N = 50$ m. However, the validity of the 2-dimensional assumption fails at peak observed flow speeds of $O(1$ m s$^{-1})$. Under such circumstances the flow may be blocked by the reef and be forced to travel around it, inducing strong vorticity at the reef edge.

Flow directed over the reef is implicated in the mechanism driving the vertical excursion of the density surface contours (isopycnals) on either side of the reef throughout the tidal cycle. Isopycnals descended rapidly on both sides of the reef in response
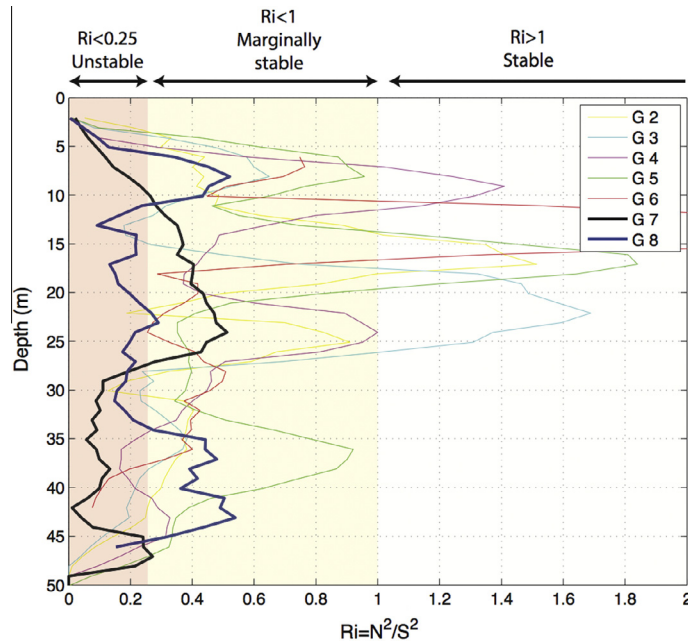
Fig. 11. Vertical profiles of the Richardson number, $Ri = N^2/S^2$, during groups 2–8 at waypoint 5 (to the south of the reef where highest sightings were recorded). The profiles obtained during groups 7 and 8, when the highest sightings were recorded, are indicated by the bold lines. Red shading represents conditions for which shear instability is expected at $Ri < 0.25$ and the yellow shading for which conditions are marginally stable ($Ri < 1$). The profiles were smoothed with a 5 point running average filter. (For interpretation of the references to colour in this figure legend, the reader is referred to the web version of this article.)
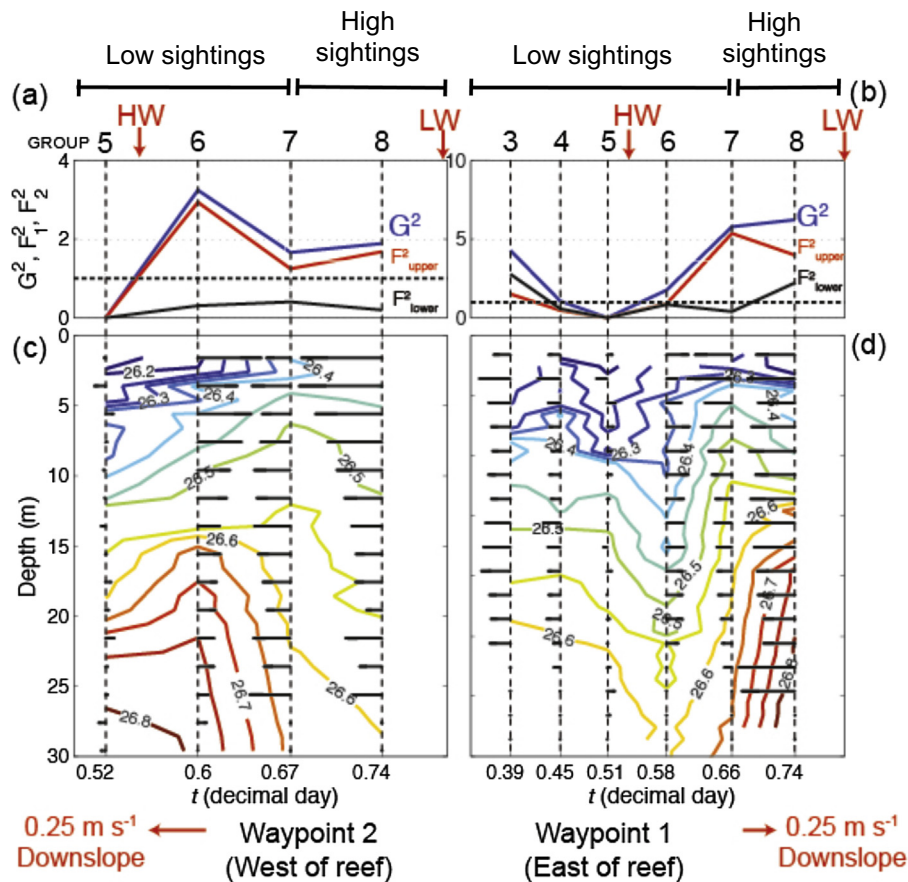
Fig. 12. (a,b) Froude numbers and (c,d) isopycnals (coloured lines) and mean U velocity vectors (black lines) at waypoints 2 and 1 on the western and eastern side of the reef respectively. Isopycnal depths are estimated from the CTD profiles conducted at the beginning and end of leg 1 for groups 3–8 (WP 1) and 5–8 (WP 2). Velocity vectors were calculated from ADCP data as mean eastward velocities over a 1-min period corresponding to the time of the CTD profile. The vectors show westward velocities when directed to the left, and eastward velocities when directed to the right. (For interpretation of the references to colour in this figure legend, the reader is referred to the web version of this article.)
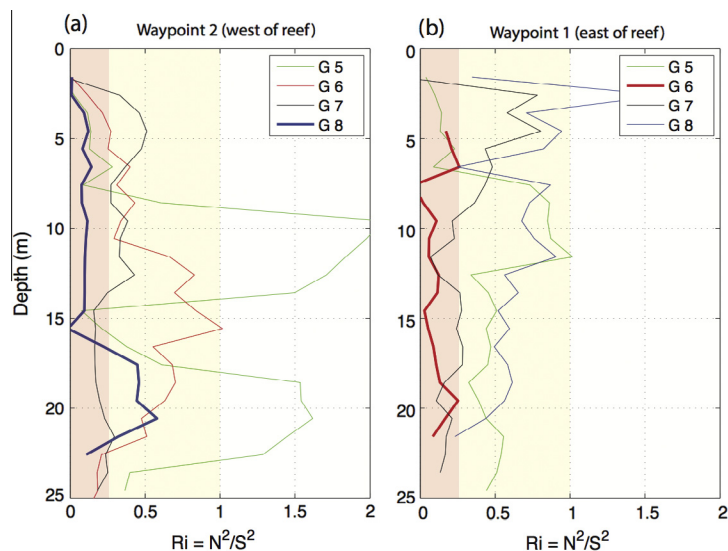
Fig. 13. Richardson number profiles during groups 5–8 for (a) WP 2 on the western side of the reef and (b) WP 1 on the eastern side. Shading is as in Fig. 11. Bold lines indicate profiles corresponding to times when isopycnals were observed to deepen rapidly on either side of the reef (group 8 at WP2, group 6 at WP1). These time periods also correspond to shear-induced instabilities detected in echo intensity, as highlighted by the black box in Fig. 8.

to currents directed down the respective side of the reef (Fig. 12). At WP1, on the eastern side of the reef, a pronounced (>10 m) depression of isopycnals occurred during group 6 as the flow was briefly (∼2 h) directed off the reef to the east (Fig. 12d). At WP2 on the western side of the reef, isopycnals similarly descended >10 m over less than 2 h between groups 7 and 8 when the currents reversed from eastward (up-slope) during the preceding groups to westward (down-slope; Fig. 12c). Thus isopycnals were depressed in the lee of the reef when defined by the orientation of the current but, following relaxation or reversal of that current, returned and even overshot by a considerable distance their initial depth. During the same period, baroclinic velocities in the upper and lower layers increased in magnitude on both sides of the reef but were orientated in opposite directions, indicating the generation of significant shear (Fig. 8). Note that black horizontal lines in Fig. 12c and d indicate the velocity measured at the end of the cross-reef section; velocities over the bank itself were significantly greater by up to a factor of 2 (Fig. S6a).

Vertical profiles of Ri provide strong evidence for the criticality of the flow to shear instability and thus the generation of turbulence at the times when the lee waves were observed on both sides of the reef (Fig. 13). CTD data were collected at both WP 1 and 2 throughout transect groups 5–8. These data show that Ri was typically <1, indicating marginal stability. However, during group 8 at WP 2 on the western side of the reef (Fig. 13a) and during group 6 at WP 1 on the eastern side (Fig. 13b); Ri < 0.25 throughout the water column indicating widespread shear instability. These times of minimum Ri correspond exactly to the period during which isopycnals were rapidly depressed on either side of the reef (Fig. 12c and d) and represent the minimum values of Ri observed throughout the survey. At WP 2 at the western side of the reef, Ri decreased continuously from group 5 until group 8 (Fig. 13a) as the lee wave was formed (Fig. 12c). Similarly at WP 1 to the east of the reef, Ri increased following group 6 (Fig. 13b) as the lee wave passed (Fig. 12d).

Cross-reef currents, estimated as U, were maximal at WP1 during group 6 and directed to the east (velocity vectors in Fig. 12c and d), thereby constituting a down-slope flow. Previous observations over isolated sills and ledges have demonstrated the generation of lee waves and, under strong flows, hydraulically supercritical conditions (e.g. Klymak and Gregg, 2004; McCabe et al., 2006).

Having potentially identified hydraulic jumps occurring at the site, we estimated the composite internal Froude number in order to assess the extent to which the flow at the reef was hydraulically controlled over the slopes to the east and west sides. Froude number was estimated as:

$$G^2 = F_1^2 + F_2^2$$

where $F^2_i = u^2_i/g'h_i$ are the internal Froude for each layer, $i = 1$ and 2, corresponding to the upper and lower layer respectively and $g' = \Delta\rho/\rho$ is the reduced gravitational acceleration(Armi, 1986). The interface between the two layers is defined by the position of the 1026.55 kg m^{-3} isopycnal. For $G^2 > 1$ the flow is supercritical and kinetic energy dominates the flow such that waves cannot propagate away, whereas for $G^2 < 1$, potential energy dominates and waves can propagate in any direction. For a given layer, supercritical flows ($F > 1$) tend to be fast and shallow, whereas subcritical flows ($F < 1$) are usually slower and deeper. When the flow changes between supercritical and subcritical regimes (e.g. when tidal currents change or flow interacts with local topography), a hydraulic jump can occur (Farmer and Armi, 1999). This is characterised by a sudden change in the layer depth and associated changes from potential to kinetic energy, usually accompanied by shear instability (Lawrence, 1990) and turbulent mixing (Moum and Nash, 2000).

Flow became supercritical (hydraulically controlled) at WP 1 at precisely the time that the depression of isopycnals was observed (G6-7, Fig. 12b and d). As the flow was previously subcritical (i.e. $G^2 < 1$) during transect groups 4 and 5, the transition to supercritical conditions is likely to have occurred in the form of a hydraulic jump as the current was briefly reversed to a downslope direction (see velocity vectors in Fig. 12d). The upper layer appears to exert the dominant hydraulic control with the corresponding Froude number, F, always larger than the lower layer F; which reached supercritical values only during groups 3 and 8 at WP 1 (Fig. 12b, black line). The rationale for the upper layer control is clear when considering the current magnitude; velocities are intensified at the surface and decrease towards the bed (as indicated by velocity vectors in Fig. 6 and 12c and d) in much the same way as depicted in Cummins et al. (2006). At WP 2 (on the western side of the reef) the lower layer F remains subcritical throughout the survey, but the upper layer flow becomes supercritical between groups 6 and

7 (Fig. 12a), approximately 1.5 h before the isopycnal depression occurs (Fig. 12c). Note that at WP2 the isopycnals deepened at the same time as the current reversed to a downslope orientation (at ∼HW +2; see velocity vectors for G6-7 in Fig. 12c). The flow around the reef thus appears to be hydraulically controlled and transitions from sub- to supercritical as it reverses to a downslope orientation on either side of the reef. The depression of isopycnals occurs at both WP 1 and 2 during tidal flows associated with low sightings (G5 & 6, Fig. 12c and d). However the subsequent recovery of the isopycnals, associated with maximum baroclinic velocities (Fig. 8), flow reversal and release of a lee wave, occurred during the tidal period with greatest porpoise sighting rates. This is particularly evident at WP1 on the eastern side of the reef, where greatest porpoise densities were recorded (Figs. 12b and d, 2).

Summary of the fine scale spatial distribution of porpoise sightings in relation to hydrodynamic features

Our findings show that porpoise sightings were clustered (Fig. 2), with greatest numbers observed in parts of study area with a south-westerly aspect, combined with moderate depth and steep topography (Fig. 3). The sighting rates were highest during periods of westward tidal flow, peaking during the strongest westward flows between approximately 2 and 6 h after HW (Figs. 5 and 7). This period of the tidal cycle is represented during groups G7 and G8 of the oceanographic survey, and was characterised by cooler (denser) water moving through the survey area and a drop in fluorescence (Fig. 9). Intriguingly, we recorded development of layered flows and water column instabilities within the area of highest porpoise sighting density (legs 3 and 4 of the ADCP transect, Fig. 1) during G7 and G8 of the oceanographic survey. The specific hydrodynamic features identified in the physical data include:

(1) Layered flow (e.g. between HW +3.5 and LW: see profiles G7 and G8 in Fig. 7a, and G8 in Fig. 7b) likely to be created by tidal-topographic interactions at the steeply sloping reef edge (velocity vectors in Fig. 6) and driven by baroclinic currents (Fig. 8).
(2) The layered flows described above were associated with mid-depth shear boundaries, for example the line of lighter colouring at mid-depth along legs 3 and 4 in Fig 6.
(3) Mid-depth shear induced instability is further evidenced during G7 and G8 by the 'billows' in the echo intensity along leg 4 of the ADCP transect (Fig. 10), and low Richardson numbers recorded at WP5 (located at the southern end of leg 4, within the core porpoise sightings area; Fig. 11). These features suggest susceptibility to shear-induced turbulence during the periods of the tidal cycle characterised by strong westward flows, when highest sighting rates were recorded throughout the visual survey.
(4) Peak sightings are closely related to the timing of hydraulically critical conditions on either side of the reef and the generation of lee waves. The waves are initially formed by the down-slope flow and then subsequently radiate away from the reef as the current reverses to an up-slope orientation. On the eastern side of the reef (at WP 1 in the core sightings area), the hydraulic jump occurs on the eastward flow, evidenced by the transition from sub- to super-critical flow during the down-slope current (Fig. 12b). The hydraulically controlled flow is associated with a depression of the isopycnals (G5-6, Fig. 12d) during the period of lowest sighting rates recorded on the eastward flood tide (∼HW −1 to HW +1, Fig. 5). The isopycnals on the eastern side of the reef were subsequently released as the tide turned back westwards (i.e. up-slope; G7-8, Fig. 12b and d). This timing cor-

responds to the tidal flows associated with the greatest porpoise sightings (∼HW +2 to LW, Fig. 5). We propose the return of the isopycnals represents the release of the lee wave at the eastern side of the reef as the flow returned to an up-slope direction.

Discussion

This study is the first to examine fine-scale (up to ∼600 m) habitat associations of harbour porpoises with reference to quantitative high-resolution hydrodynamic data (1-m vertical resolution and 2-s ensemble interval) collected within an identified hotspot for the species. Harbour porpoise sightings recorded at the Runnel-stone Reef during this study were not distributed uniformly across the survey area (Fig. 2). Higher relative densities were associated with moderate depths and steeply sloping topography, in particular around the southeastern reef margins (Fig. 3). The importance of this part of the survey area has also been identified in boat-based studies (Fig. S3), and in passive acoustic data collected at three sites within the survey area using CPODs deployed during the 2010 survey season (Jones, 2012). We have linked the fine-scale spatio-temporal variability in porpoise surface sightings to hydrodynamic features associated with predictable tidal time-scales. These include tidal flow velocity (Figs. 7 and 8), shear (Fig. 6), shear-induced instabilities (Figs. 10, 11 and 13) and changes in water column properties (Figs. 9 and 12).

Our results provide insights into the fine-scale functional mechanisms driving the physical habitat associations that are often reported in broader extent and coarser scale studies on this species. Previous studies have identified links between porpoise sightings and areas of specific physical habitat, such as moderate depth (Northridge et al., 1995; Goodwin and Speedie, 2008; Marubini et al., 2009), high slope (Pierpoint, 2008; Booth et al., 2013) and tidal variables (Johnston et al., 2005; Embling et al., 2010; Isojunno et al., 2012). However, the physical variables identified in these studies are generally recognised as proxies for underlying drivers (e.g. Isojunno et al., 2012; Booth et al., 2013) and few studies have been able to provide quantitative data on the potential physical mechanisms at the root of these habitat associations (De Boer et al., 2014).

We have demonstrated that the current regime at the Runnelstone Reef was sufficient to generate hydraulic jumps during across-reef flows. Specifically there was transition from subcritical to supercritical hydraulic flow at the eastern side of the reef, just prior to the time of maximum sightings which was associated with the subsequent development of a lee wave as the flow reversed upslope (westwards). Estimates of the Richardson number from WP1 (at the east side of the reef) confirm that the water column was highly susceptible to shear instability during the periods of upper layer supercritical flow, experienced at times of the tidal cycle associated with greatest numbers of sightings. Our results suggest that the high numbers of porpoises sighted during westward flows were exploiting periods during which lee waves were formed along the sloping margins of the Runnelstone Reef, and that these aspects of the flow field arose as a result of the influence of bathymetric features on the tidal currents (tidal-topographic interaction); leading to baroclinic flow, hydraulic jumps and lee waves.

Given the oscillatory nature of the flow and the wide range of current speeds and stratification experienced at the site, we consider that the flow field is most likely to generate all of the above hydrodynamic features, depending primarily on the strength of the currents. The regime appears to be similar to that depicted in Nash and Moum (2001, their Fig. 5), for which hydraulic jumps and lee waves form on the downstream side of the ridge and low Richardson number shear instabilities form over the ridge due to the highly sheared currents. Our observations, taken from a single

tidal cycle in the middle of the spring-neap phase, suggest that lee waves are a common feature at the reef and lead to enhanced shear and associated turbulent mixing. Pronounced curvature in the flow field offshore of the reef further indicates an increase in vorticity and likely flow separation, which other studies have shown will produce a lee eddy on the downstream side of the headland. The definitive link between these well-defined processes and the porpoise activity requires further targeted research but the timing of the hydrodynamic processes and porpoise sightings appears not to be coincidental.

We only recorded the simultaneous velocity and CTD measurements required for the computation of Froude number (F) on either side of the Runnelstone Reef (at WP1 and 2 on the east and west sides respectively). Velocities over the shallower reef top are much higher (Fig. S6) and as a result we would expect significantly higher values of F in these areas, where turbulence generation is more pronounced (Fig. 6, leg 1). Therefore, the values of F we present can be considered a lower limit.

We expect that the localised oceanographic features identified in our study area lead to improved foraging opportunities for prey fish, and subsequently porpoises, at specific areas within the Runnelstone Reef survey site at temporal scales of hours to days. Johnston and Read (2007) identified meso-scale bio-physical links between porpoises and hydrodynamics in the Bay of Fundy, where the evolution of tidally induced vertical shear boundaries around small eddies created by an island wake was associated with high concentrations of sound-scatterers (zooplankton and fish). They thus provide direct evidence for increased porpoise foraging opportunities associated with shear; however it should be noted that their study was over a larger spatial scale than our study; and different physical processes, such as secondary flows, may have influenced their findings (Johnston and Read, 2007). The small scale of Runnelstone Reef compared to the Bay of Fundy, and the short (tidal) timescales of variability in the current field suggest that the influence of the topography may be more relevant to prey availability rather than prey abundance (Embling et al., 2013; Thorne and Read, 2013). Such a distinction may also explain why the highest sightings were made at a time during the oceanographic survey when chlorophyll reached minimum values (Fig. 9), thereby suggesting that the factors other than the abundance of phytoplankton are important in driving porpoise foraging distribution at the site.

How higher predators key into prey aggregations is not well understood but is assumed to be associated with maximising foraging efficiency as described by Houghton et al. (2006) and Sims et al. (2008). It has also been noted that the distribution of top predators at a fine-scale may be more influenced by the predictability or energy value of prey, rather than prey abundance *per se* (Grémillet et al., 2008; Benoit-Bird et al., 2013), and that memory of profitable areas can also play an important role in deterministic selection of foraging habitat (Nabe-Nielsen et al., 2013; Regular et al., 2013).

Recent studies by Scott et al. (2010, 2013) and Embling et al. (2012, 2013) have attempted to elucidate the biophysical links between current flow and marine species distribution at a small-scale in shelf seas. Their studies provide empirical evidence of links between tidal forcing, chlorophyll, fish and seabirds. Specifically, Embling et al. (2013) studied fish behaviour in response to hydrodynamics at Jones Bank in the Celtic Sea. They found that internal waves created during hydraulically controlled flows over the shallow sea bank (see also Palmer et al., 2013) acted to concentrate both zooplankton and zooplanktivorous fish close to the surface. Similar results were also reported in Embling et al. (2012). Such biophysical links may also be acting within our study area, leading to prey fish aggregation and favourable foraging conditions for porpoises.

The spatial and temporal consistency of the flow features identified in the ADCP survey, as well as the causative biophysical links between them and the distribution of porpoises, require further investigation. A repeated ADCP survey over the transect route, carried out at a variety of periods within the spring-neap cycle, would provide more robust characterisation of tidal-topographically controlled hydrodynamics at the site. Collection of bio-acoustic data, using hydroacoustic tools such as the EK60 echosounder, along with collection of plankton samples during the ADCP transect would add valuable direct biological evidence of spatial and/or temporal concentration of prey at the survey site, which is missing from this analysis.

The links that we have identified between fine-scale porpoise distribution and ephemeral, but predictable, tidal-topographic flow features are likely to be overlooked in studies covering a larger area and with less intensive temporal survey coverage (Wiens, 1989; Isojunno et al., 2012). However, the results must be taken in the context of the limited spatial and temporal coverage of the visual survey data. In addition, as with all visual survey data, the distribution of surface sightings of porpoises is assumed to be representative of habitat usage throughout the water column.

Conservation applications

UK waters are home to a significant number of Europe's harbour porpoises (Hammond et al., 1995, 2002; Hammond, 2006), but there is currently only a single SAC in UK waters where the species is identified as a 'qualifying feature' (N.I.E.A., 2010, 2011). The guidelines for site selection of proposed porpoise SACs state that the area should contain key sites that are used regularly by high numbers of the species, and they "must be clearly identifiable areas representing the physical and biological factors essential to the species' life and reproduction" (Article 4 of the Council Directive 92/43/EEC). In order for these sites to be identified, the species' interactions with their physical and biological environment must be better understood. Our research, and other recent studies, indicate that there are complex interactions between static and dynamic environmental variables in the marine environment, and that sole reliance on static physical features for the identification of key habitats may not accurately capture the complexities of the biophysical interactions involved in habitat selection (e.g. Johnston et al., 2005; Scott et al., 2010, 2013; Embling et al., 2012; Isojunno et al., 2012; Embling et al., 2013; Thorne and Read, 2013; De Boer et al., 2014). In addition, information on the interaction of porpoises with fine-scale flow features is necessary in order to understand the possible effects of the installation of tidal turbines or wave energy arrays, which may have the potential to exclude porpoises from areas of key foraging habitat in tidally dynamic areas, or alter localised flows (Dolman and Simmonds, 2010; Simmonds and Brown, 2010; Shields et al., 2011).

Conclusion

In line with our stated aims, the data presented in this study build upon the limited research into the underlying biophysical drivers of fine-scale porpoise distribution within a known hotspot. We provide new insights into specific hydrodynamic features, produced through tidal forcing, that may be important for creating foraging opportunities at a local scale. These spatially and temporally predictable dynamic habitats are likely to be especially important for porpoises due to their small size, high metabolism and requirement for regular feeding. Although aspects of the fine-scale biophysical interactions between harbour porpoises and their immediate environment remain unanswered, this study represents an increase in knowledge, and highlights the complexities of the relationship between the animals and their physical habitat.

Increasing our understanding of habitat associations and, perhaps more importantly, the mechanistic links between oceanographic variables and top predator distribution, is a key research area within the context of vulnerable marine species protection. Description of fine-scale species distributions can provide important information on key habitats, trends in variation of habitat use, and animal-environment interactions, which give insight into potential drivers of distribution. In addition, our research highlights the value of visual monitoring at key hotspot locations where regular boat-based transect surveys are excluded by conditions, other users of the sea, or prohibitive costs. It is hoped that the data presented here will help to direct future multidisciplinary research, focussed on the fine-scale biophysical drivers of marine vertebrate distribution within hotspot areas, in order to better understand why these particular sites prove especially attractive.

Acknowledgments

Appendix A. Supplementary material

Supplementary data associated with this article can be found, in the online version, at http://dx.doi.org/10.1016/j.pocean.2014.08.002.

References

Armi, L., 1986. The hydraulics of two flowing layers with different densities. Journal of Fluid Mechanics 163, 27–58.

Baddeley, A., Turner, R., 2005. Spatstat: an R package for analyzing spatial point patterns. Journal of Statistical Software 12, 1548–7760.

Benoit-Bird, K.J., Battaile, B.C., Heppell, S.A., Hoover, B., Irons, D., Jones, N., Kuletz, K.J., Nordstrom, C.A., Paredes, R., Suryan, R.M., Waluk, C.M., Trites, A.W., 2013. Prey patch patterns predict habitat use by top marine predators with diverse foraging strategies. PLoS ONE 8.

Bertrand, A., Gerlotto, F., Bertrand, S., Gutiérrez, M., Alza, L., Chipollini, A., Díaz, E., Espinoza, P., Ledesma, J., Quesquén, R., Peraltilla, S., Chavez, F., 2008. Schooling behaviour and environmental forcing in relation to anchoveta distribution: an analysis across multiple spatial scales. Progress in Oceanography 79, 264–277.

Beyer, H., 2012. Geospatial Modelling Environment (version 0.6.0.0). Spatial Ecology LLC.

Booth, C.G., Embling, C., Gordon, J., Calderan, S.V., Hammond, P.S., 2013. Habitat preferences and distribution of the harbour porpoise Phocoena phocoena west of Scotland. Marine Ecology Progress Series 478, 273–285.

Börger, L., Franconi, N., De Michele, G., Gantz, A., Meschi, F., Manica, A., Lovari, S., Coulson, T., 2006. Effects of sampling regime on the mean and variance of home range size estimates. Journal of Animal Ecology 75, 1393–1405.

Bowman, A.W., Azzalini, A., 2010. R package 'sm': nonparametric smoothing methods (version 2.2-4).

Brereton, T., MacLeod, C.D., Wall, D., MacLeod, K., Cermeno, P., Curtis, D., Zanderink, F., Benson, C., Osinga, N., Martin, C., Pinn, E., 2007. Monitoring Cetaceans in UK and Adjacent Waters: Current and Potential Uses of Atlantic Research Coalition (ARC) Data. Atlantic Research Coalition.

Brodie, P.F., 1995. The Bay of Fundy/Gulf of Maine harbour porpoise (Phocoena phocoena): some considerations regarding species interactions, energetics density dependence and by-catch. In: Bjorge, A., Donovan, G.P. (Eds.), Special Issue, 16: Biology of Phocoenids. International Whaling Commission, Cambridge, pp. 181–187.

Buckland, S.T., Anderson, D.R., Burnham, K.P., Laake, J.L., Borchers, D.L., Thomas, L., 2001. Introduction to Distance Sampling: Estimating Abundance of Biological Populations. Oxford University Press, Oxford, UK.

Buckland, S.T., Anderson, D.R., Burnham, K.P., Laake, J.L., Borchers, D.L., Thomas, L., 2004. Advanced Distance Sampling. Oxford University Press, Oxford, UK.

Buckland, S.T., Marsden, S.J., Green, R.E., 2008. Estimating bird abundance: making methods work. Bird Conservation International 18, S91–S108.

Burnham, K.P., Andersen, D.R., 2002. Model Selection and Multimodel Inference. A Practical Information-theoretic Approach. Springer-Verlag, New York.

Cummins, P.F., Armi, L., Vagle, S., 2006. Upstream internal hydraulic jumps. Journal of Physical Oceanography 36, 753–769.

De Boer, M.N., Saulino, J.T., 2008. Winter distribution and density of small cetaceans in the inshore fishing grounds off southwest England. Annual Conference of the European Cetacean Society. Egmond aan Zee, The Netherlands, pp. 229 (Abstract S-206).

De Boer, M.N., Simmonds, M.P., Reijnders, P.J.H., Aarts, G., 2014. The influence of topographic and dynamic cyclic variables on the distribution of small cetaceans in a shallow coastal system. PLoS ONE 9, e86331.

Development Core Team, R., 2011. R: A Language and Environment for Statistical Computing. R Foundation for Statistical Computing, Vienna, Austria.

Dolman, S., Simmonds, M., 2010. Towards best environmental practice for cetacean conservation in developing Scotland's marine renewable energy. Marine Policy 34, 1021–1027.

Embling, C.B., Gillibrand, P.A., Gordon, J., Shrimpton, J., Stevick, P.T., Hammond, P.S., 2010. Using habitat models to identify suitable sites for marine protected areas for harbour porpoises (Phocoena phocoena). Biological Conservation 143, 267–279.

Embling, C.B., Illian, J., Armstrong, E., van der Kooij, J., Sharples, J., Camphuysen, C.J., Scott, B.E., 2012. Investigating fine-scale spatio-temporal predator-pey patterns in dynamic marine ecosystems: a functional data analysis approach. Journal of Applied Ecology 49, 481–492.

Embling, C.B., Sharples, J., Armstrong, E., Palmer, M.R., Scott, B.E., 2013. Fish behaviour in response to tidal variability and internal waves over a shelf sea bank. Progress in Oceanography.

Evans, P., Anderwald, P., Baines, M.E., 2003. UK Cetacean Status Review. Report to English Nature and Countryside Council for Wales. Oxford: Seawatch Foundation, p. 160.

Farmer, D.M., Armi, L., 1999. Stratified flow over topography: the role of small scale entrainment and mixing in flow reestablishment. Proceedings of the Royal Society of London, Series A 455, 3221–3258.

Fauchald, P., Erikstad, K.E., 2002. Scale-dependent predator-prey interactions: the aggregative response of seabirds to prey under variable prey abundance and patchiness. Marine Ecology Progress Series 231, 279–291.

Geyer, W.R., 1993. Three-dimensional tidal flow around headlands. Journal of Geophysical Research: Oceans 98, 955–966.

Goodwin, L., Speedie, C., 2008. Relative abundance, density and distribution of the harbour porpoise (Phocoena phocoena) along the west coast of the UK. Journal of the Marine Biological Association of the United Kingdom 88, 1221–1228.

Grémillet, D., Lewis, S., Drapeau, L., Van Der Lingen, C.D., Huggett, J.A., Coetzee, J.C., Verheye, H.M., Daunt, F., Wanless, S., Ryan, P.G., 2008. Spatial match–mismatch in the Benguela upwelling zone: should we expect chlorophyll and sea-surface temperature to predict marine predator distributions? Journal of Applied Ecology 45, 610–621.

Hammond, P., 2006. Small Cetaceans in the European Atlantic and North Sea. In P. Hammond (Ed.), LIFE Project. St. Andrews: Sea Mammal Research Unit, University of St. Andrews, p. 55.

Hammond, P.S., Benke, H., Berggren, P., Borchers, P., Buckland, S.T., Collet, A., Heide-Jorgensen, M.P., Heimlich-Boran, S., Hiby, A.R., Leopold, M.F., Oien, N., 1995. Distribution and Abundance of the Harbour Porpoise and Other Small Cetaceans in the North Sea and Adjacent Waters. SCANS, p. 240.

Hammond, P.S., Berggren, P., Benke, H., Borchers, D.L., Collet, A., Heide-Jorgensen, M.P., Heimlich, S., Hiby, A.R., Leopold, M.F., Oien, N., 2002. Abundance of harbour porpoise and other cetaceans in the North Sea and adjacent waters. Journal of Applied Ecology 39, 361–376.

Hammond, P.S., Macleod, K., Berggren, P., Borchers, D.L., Burt, L., Cañadas, A., Desportes, G.V., Donovan, G.P., Gilles, A., Gillespie, D., Gordon, J., Hiby, L., Kuklik, I., Leaper, R., Lehnert, K., Leopold, M., Lovell, P., Øien, N., Paxton, C.G.M., Ridoux, V., Rogan, E., Samarra, F., Scheidat, M., Sequeira, M., Siebert, U., Skov, H., Swift, R., Tasker, M.L., Teilmann, J., Van Canneyt, O., VÃzquez, J.A., 2013. Cetacean abundance and distribution in European Atlantic shelf waters to inform conservation and management. Biological Conservation 164, 107–122.

Hastie, T.J., Tibshirani, R.J., 1990. Generalised Additive Models. Chapman and Hall/CRC, New York.

Herr, H., Fock, H.O., Siebert, U., 2009. Spatio-temporal associations between harbour porpoise Phocoena phocoena and specific fisheries in the German Bight. Biological Conservation 142, 2962–2972.

Houghton, J.D.R., Doyle, T.K., Wilson, M.W., Davenport, J., Hays, G.C., 2006. Jellyfish aggregations and leatherback turtle foraging patterns in a temperate coastal environment. Ecology 87, 1967–1972.

Hunt, J.C.R., Snyder, W.H., 1980. Experiments on stably and neutrally stratified flow over a model three-dimensional hill. Journal of Fluid Mechanics 96, 671–704.

Isojunno, S., Matthiopoulos, J., Evans, P.G.H., 2012. Harbour porpoise preferences: robust spatio-temporal inferences from opportunistic data. Marine Ecology Progress Series 448, 155–170.

Johnston, D.W., Read, A.J., 2007. Flow-field observations of a tidally driven island wake used by marine mammals in the Bay of Fundy, Canada. Fisheries Oceanography 16, 422–435.

Johnston, D.W., Westgate, A.J., Read, A.J., 2005. Effects of fine-scale oceanographic features on the distribution and movements of harbour porpoises Phocoena phocoena in the Bay of Fundy. Marine Ecology-Progress Series 295, 279–293.

Jones, A., 2012. PhD Thesis: The spatio-temporal distribution and habitat associations of marine mega-vertebrates off southwest UK. Faculty of Natural and Earth Sciences, Ocean and Earth Science. Southampton: University of Southampton, p. 329.

Kai, E.T., Rossi, V., Sudre, J., Weimerskirch, H., Lopez, C., Hernandez-Garcia, E., Marsac, F., Garcon, V., 2009. Top marine predators track Lagrangian coherent structures. Proceedings of the National Academy of Sciences of the United States of America 106, 8245–8250.

Klymak, J.M., Gregg, M.C., 2004. Tidally generated turbulence over the knight inlet sill. Journal of Physical Oceanography 34, 1135–1151.

Koopman, H., 1998. Topographical distribution of the blubber of harbour porpoises (Phocoena phocoena). Journal of Mammology 79, 260–270.

Lawrence, G.A., 1990. On the hydraulics of Boussinesq and non-Boussinesq two-layered flows. Journal of Fluid Mechanics 215, 457–480.

Leeney, R.H., Amies, R., Broderick, A.C., Witt, M.J., Loveridge, J., Doyle, J., Godley, B.J., 2008. Spatio-temporal analysis of cetacean strandings and bycatch in a UK fisheries hotspot. Biodiversity and Conservation 17, 2323–2338.

Legendre, P., Legendre, L., 2012. Numerical Ecology. Elsevier.

Lockyer, C., 2007. All creatures great and smaller: a study in cetacean life history energetics. Journal of the Marine Biological Association of the UK 87, 1035–1045.

Lueck, R.G., Lu, Y., 1997. The logarithmic layer in a tidal channel. Continental Shelf Research 17, 1785–1801.

Marubini, F., Gimona, A., Evans, P.G.H., Wright, P.J., Pierce, G.J., 2009. Habitat preferences and interannual variability in occurrence of the harbour porpoise Phocoena phocoena off northwest Scotland. Marine Ecology-Progress Series 381, 297–310.

McCabe, R.M., MacCready, P., Pawlak, G., 2006. Form drag due to flow separation at a Headland. Journal of Physical Oceanography 36, 2136–2152.

Mikkelsen, L., Mouritsen, K.N., Dahl, K., Teilmann, J., Tougaard, J., 2013. Re-established stony reef attracts harbour porpoises Phocoena phocoena. Marine Ecology-Progress Series 481, 239–248.

Miles, J., 1961. On the stability of heterogeneous shear flows. Journal of Fluid Mechanics 104.

Moum, J.N., Nash, J.D., 2000. Topographically-induced drag and mixing at a small bank on the continental shelf. Journal of Physical Oceanography 30, 2049–2054.

Myers, N., 1990. The biodiversity challenge: expanded hotspots analysis. Environmentalist 8, 1–20.

N.I.E.A., 2010. Inshore Special Area of Conservation: Skerries and Causeway SAC Selection Assesment. Belfast, NI: Northern Ireland Environment Agency, p. 38.

N.I.E.A., 2011. Inshore Special Area of Conservation: Skerries and Causeway Conservation Objectives and Advice on Operations. Northern Ireland Environment Agency, p. 18.

Nabe-Nielsen, J., Tougaard, J., Teilmann, J., Lucke, K., Forchhammer, M.C., 2013. How a simple adaptive foraging strategy can lead to emergent home ranges and increased food intake. Oikos.

Nash, J.D., Moum, J.N., 2001. Internal hydraulic flows on the continental shelf: high drag states over a small bank. Journal of Geophysical Research: Oceans 106, 4593–4611.

Nichols, J.D., Hines, J.E., Sauer, J.R., Fallon, F.W., Fallon, J.E., Heglund, P.J., 2000. A Double-observer approach for estimating detection probability and abundance from point counts. The Auk 117, 393–408.

Northridge, S.P., Tasker, M.L., Webb, A., Williams, J.M., 1995. Distribution and relative abundance of harbour porpoises (Phocoena phocoena L.), white beaked dolphins (Lagenorhynchus albirostris Gray) and minke whales (Balaenoptera acutorostrata Lacepede) around the British Isles. ICES Journal of Marine Science 52, 55–66.

Oksanen, J., Blanchet, F.G., Kindt, R., Legendre, P., Minchin, P.R., O'Hara, R.B., Simpson, G.L., Solymos, P., Stevens, M.H.H., Wagner, H., 2013. vegan: Community Ecology Package. R Package Version 2.0-7.

Palmer, M.R., Inall, M.E., Sharples, J., 2013. The physical oceanography of Jones Bank: a mixing hotspot in the Celtic Sea. Progress in Oceanography 117, 9–24.

Pierpoint, C., 2008. Harbour porpoise (Phocoena phocoena) foraging strategy at a high energy, near-shore site in south-west Wales, UK. Journal of the Marine Biological Association of the United Kingdom 88, 1167–1173.

Pikesley, S.K., Witt, M.J., Hardy, T., Loveridge, J., Loveridge, J., Williams, R., Godley, B.J., 2012. Cetacean sightings and strandings: evidence for spatial and temporal trends? Journal of the Marine Biological Association of the UK 92, 33.

Powell, R.A., 2000. Animal Home Ranges and Territories and Home Range Estimators. In: Boitani, L., Fuller, T.K. (Eds.), Research Techniques in Animal Ecology. Columbia University Press, New York, pp. 65–110.

Proctor, R., Bell, C., Eastwood, L., Holt, J.T., Prandle, D., Young, E.F., 2004. UK Marine Renewable Energy Atlas: Phase 2 - POL contribution. Proudman Oceanographic Laboratory, Internal Document, No 163, 26 p.

Read, A.J., Westgate, A.J., 1997. Monitoring the movements of harbour porpoises (Phocoena phocoena) with satellite telemetry. Marine Biology 130, 315–322.

Regular, P.M., Hedd, A., Montevecchi, W.A., 2013. Must marine predators always follow scaling laws? Memory guides the foraging decisions of a pursuit-diving seabird. Animal Behaviour 86, 545–552.

Reid, J.B., Evans, P.G.H., Northridge, S.P., 2003. Atlas of Cetacean Distribution in North-west European Waters. Peterborough: JNCC, p. 75.

Roughan, M., Mace, A.J., Largier, J.L., Morgan, S.G., Fisher, J.L., Carter, M.L., 2005. Subsurface recirculation and larval retention in the lee of a small headland: a variation on the upwelling shadow theme. Journal of Geophysical Research: Oceans 110, C10027.

Russell, R.W., Hunt, G.L., Coyle, K.O., Cooney, R.T., 1992. Foraging in a fractal environment: spatial patterns in a marine predator-prey system. Landscape Ecology 7, 195–209.

Santos, M.B., Pierce, G.J., Learmonth, J.A., Reid, R.J., Ross, H.M., Patterson, I.A.P., Reid, D.G., Beare, D., 2004. Variability in the diet of harbor porpoises (Phocoena phocoena) in Scottish waters 1992–2003. Marine Mammal Science 20, 1–27.

Scott, B.E., Sharples, J., Ross, O.N., Wang, J., Pierce, G.J., Camphuysen, C.J., 2010. Sub-surface hotspots in shallow seas: fine-scale limited locations of top predator foraging habitat indicated by tidal mixing and sub-surface chlorophyll. Marine Ecology Progress Series 408, 207–226.

Scott, B.E., Webb, A., Palmer, M.R., Embling, C.B., Sharples, J., 2013. Fine scale bio-physical oceanographic characteristics predict the foraging occurrence of contrasting seabird species; Gannet (Morus bassanus) & Storm Petrel (Hydrobates pelagicus). Progress in Oceanography.

Shields, M.A., Woolf, D.K., Grist, E.P.M., Kerr, S.A., Jackson, A.C., Harris, R.E., Bell, M.C., Beharie, R., Want, A., Osalusi, E., Gibb, S.W., Side, J., 2011. Marine renewable energy: the ecological implications of altering the hydrodynamics of the marine environment. Ocean & Coastal Management 54, 2–9.

Simmonds, M.P., Brown, V.C., 2010. Is there a conflict between cetacean conservation and marine renewable-energy developments? Wildlife Research 37, 688–694.

Sims, D.W., 2003. Tractable models for testing theories about natural strategies: foraging behaviour and habitat selection of free-ranging sharks. Annual Symposium of the Fisheries-Society-of-the-British-Isles. Norwich, England, pp. 53–73.

Sims, D.W., Southall, E.J., Humphries, N.E., Hays, G.C., Bradshaw, C.J.A., Pitchford, J.W., James, A., Ahmed, M.Z., Brierley, A.S., Hindell, M.A., Morritt, D., Musyl, M.K., Righton, D., Shepard, E.L.C., Wearmouth, V.J., Wilson, R.P., Witt, M.J., Metcalfe, J.D., 2008. Scaling laws of marine predator search behaviour. Nature 451, pp. 1098–U1095.

Stephens, D.W., Krebs, J.R., 1986. Foraging Theory. Princeton University Press, Princeton, USA.

Sveegaard, S., 2011. Spatial and temporal distribution of harbour porpoises in relation to their prey. National Environment Research Institute (NERI) Department for Arctic Environment, Vol. PhD. Roskilde, Denmark: Aarhus University, p. 128.

Thorne, L.H., Read, A.J., 2013. Fine-scale biophysical interactions drive prey availability at a migratory stopover site for Phalaropus spp. in the Bay of Fundy, Canada. Marine Ecology Progress Series 2013, 261–273.

van Haren, H., 2009. Using high sampling-rate ADCP for observing vigorous processes above sloping [deep] ocean bottoms. Journal of Marine Systems 77, 418–427.

van Haren, H., Gostiaux, L., 2010. A deep-ocean Kelvin–Helmholtz billow train. Geophysical Research Letters 37, L03605.

Veness, C., 2012. Calculate Distance, Bearing and more Between Latitude/longitude Points, vol. 2012.

Watts, P., Gaskin, D.E., 1985. Habitat index analysis of the harbour porpoise (Phocoena phocoena) in the southern coastal Bay of Fundy, Canada. Journal of Mammology 66, 733–744.

Wiens, J.A., 1989. Spatial scaling in ecology. Functional Ecology 3, 385–397.

Witt, M.J., Sheehan, E.V., Bearhop, S., Broderick, A.C., Conley, D.C., Cotterell, S.P., Crow, E., Grecian, W.J., Halsband, C., Hodgson, D.J., Hosegood, P., Inger, R., Miller, P.I., Sims, D.W., Thompson, R.C., Vanstaen, K., Votier, S.C., Attrill, M.J., Godley, B.J., 2012. Assessing wave energy effects on biodiversity: the Wave Hub experience. Philosophical Transactions of the Royal Society A: Mathematical, Physical and Engineering Sciences 370, 502–529.

Wood, S.N., 2006. Generalised Additive Models: An Introduction with R. Chapman and Hall/CRC, Florida.

Zuur, A.F., Ieno, E.N., Smith, G.M., 2007. Analysing Ecological Data. Springer, New York, USA.

Zuur, A.F., Ieno, E.N., Walker, N.J., Saveliev, A.A., Smith, G.M., 2009. Mixed Effects Models and Extensions in Ecology with R. Springer, New York.